# THE EFFECT OF ORGANIC SOLVENTS ON SOL-GEL HYDROXYAPATITE AND ITS APPLICATION AS BIOCOATING

by

DORNA HAKIMIMEHR

B.A.Sc., TEHRAN UNIVERSITY OF SCIENCE AND TECHNOLOGY, Iran, 1999

A THESIS SUBMITTED IN PARTIAL FULFILMENT OF
THE REQUIREMENTS FOR THE DEGREE OF

MASTER OF APPLIED SCIENCE

in

THE FACULTY OF GRADUATE STUDIES

(Department of Metals and Materials Engineering)

We accept this thesis as conforming
to the required standard

THE UNIVERSITY OF BRITISH COLUMBIA

October 2001

Department of Metals and Materials Engineering

The University of British Columbia
Vancouver, Canada

Date oct. 11 /2001

**ABSTRACT**

Hydroxyapatite (HAp) is widely used by the biomedical industry due to its excellent biocompatibility. The sol-gel process offers a relatively low temperature procedure to produce hydroxyapatite powders and thin films (<1μm). The focus of the present study is to investigate the effect of different organic solvents (methanol, ethanol, and propanol) on the sol-gel HAp in the system of triethyl phosphite and calcium nitrate. X-ray diffraction analysis, thermal gravimetric analysis, differential thermal analysis, and scanning electron microscopy (SEM) are used to investigate the phase evolution and the morphology of the HAp produced in this sol-gel system. Our results show that different organic solvents induce different HAp formation pathway. In methanol and propanol-based systems HAp forms as a result of transformation of intermediate crystalline calcium phosphate phases (such as $Ca_3(PO_4)_2$ and $Ca_2P_2O_7$). Formation of HAp in ethanol-based system is attributed to crystallization from an amorphous, intermediate apatite phase.

Titanium substrates were coated using the HAp sol. IR spectroscopy of the coatings revealed that carbonated hydroxyapatite is present in the coating, which is similar to that of the natural bone. In-vitro bioactivity test confirmed the bioactive nature of the coatings while no apparent difference was observed in the bioactivity of the coatings obtained from different solvent systems.

The type of solvent, concentration of the solution, and heat treatment time affect the quality of the coatings on stainless steel wires. The coatings obtained from low concentration (1M) methanol-based solution, heat treated at 500°C for a period of 10 minutes were the most satisfactory.

Coronary stents were also coated with HAp using this sol-gel system. The coating remained on the stent after the expansion of the stent using an angioplasty balloon.

## TABLE OF CONTENTS

## LIST OF FIGURES

## AKNOWLEDGMENTS

I would like to thank Tom Troczynski for his supervision of this project and also Dean-Mo liu for sharing his knowledge of this field with me.
I would also like to thank MIVI technologies and NSERC for funding the current study.

# CHAPTER 1
# INTRODUCTION

Ceramics and glasses have been used in health-care industry for a long time. The main advantages of ceramics in medical applications are their resistance to microbial attack, pH changes, solvent conditions and temperature. They have also been applied in dentistry and as a hard tissue replacement in musculo-skeletal systems such as bone and teeth. However their main application remains to be as bioactive coatings on various prostheses in order to add bioactive characteristics to the otherwise inert implants.

Sol-gel processing seems to be one of the best methods to produce thin film coatings at low temperatures, with controlled microstructures. Lower temperature processing is the most attractive characteristic of the sol-gel technique in biomedical applications, as high temperature processing of the coating might adversely affect the mechanical properties of the substrate. The microstructure and phase development of the coating, that affect coating's bioactivity as well as its long-term performance in biological environment, are well controlled in the sol-gel process.

Process development and characterization of hydroxyapatite (HAp) bioceramics through sol-gel has been the main focus of this work. The knowledge thus obtained is applied in coating several medical substrates. Some of these attempts, such as HAp coating on coronary stents, are novel applications of hydroxyapatite coatings.

## 1.1 Biomaterials

A biomaterial is "any material used to replace or restore function to body tissue and is continuously or intermittently in contact with body fluids" [1]. Biomaterials are divided in to different categories according to the responses they elicit in the body, including biologically inert, porous, resorbable, and bioactive materials. Bioactive materials "elicit a specific biological response at the interface of the material which results in the formation of a bond between the tissues and the material [2]".

### 1.1.1 Hydroxyapatite

Calcium phosphate materials, and hydroxyapatite (HAp) in particular, are among the most widely used biomaterials in biomedical applications. Hydroxyapatite is the most appropriate ceramic material for artificial teeth or bones due to its excellent biocompatibility and bioactivity. HAp interacts with body fluids through complex dissolution-reprecipitation process. In a simplified description [2], a HAp implant, or an implant coated with HAp, will produce a local decrease of pH (an "acidic condition") at the implant area upon introduction to the biological environment. This acidic condition will promote the dissolution of the HAp, i.e. release of $Ca^{2+}$, $PO_4^{3-}$ and $HPO_4^{2-}$, which will saturate the microenvironment with calcium phosphates. This saturation leads back to deposition of a layer of carbonate-containing apatite through seeded growth on the HAp crystals. The rate of formation of this carbonated hydroxyapatite determines the extent of the bioactivity of the implant and is controlled by the crystallinity of the synthetic HAp. The dissolution of HAp is also governed by chemical composition, crystal structure and microporosity of the material [2].

Despite excellent bioactivity and biocompatibility of hydroxyapatite, its poor mechanical properties restrict its applications to powders (e.g. bone loss fillers), coatings on metallic substrates, or implants under very low loads (e.g. inner ear implants [3]). Coated implants combine good mechanical strength of the metallic substrate with excellent bioactive properties of the HAp. Uncoated metallic implants do not integrate with the bone and are encapsulated by dense fibrous tissue, which prevents proper stress distribution and will cause implant loosening [4]. In the case of HAp coated prostheses, the bone will integrate with the implant providing a stable fixation [5]. The HAp coating will also prevent the fibrous tissue encapsulation of the implant while decreasing the release of metal ions from the implant into the body and protecting the metal surface from environmental attack [6].

Many techniques have been adopted and studied in order to coat a HAp layer on a metallic substrate. Plasma spraying [7], hot isostatic pressing [8], ion beam deposition [9], flame spraying [10], and electrochemical deposition [11] are among the many. Sol-gel processing offers an alternative process in coating metallic implants. The

advantages of this process are the low temperature synthesis and microstructural control.

### 1.2 Sol-gel process

Sol-gel is a multi-step process in which a colloidal solution is prepared through hydrolysis of a suitable precursor. The starting precursor in the sol-gel process is usually a metallic alkoxide dissolved in alcohol, and then hydrolysed through controlled addition of water [12].

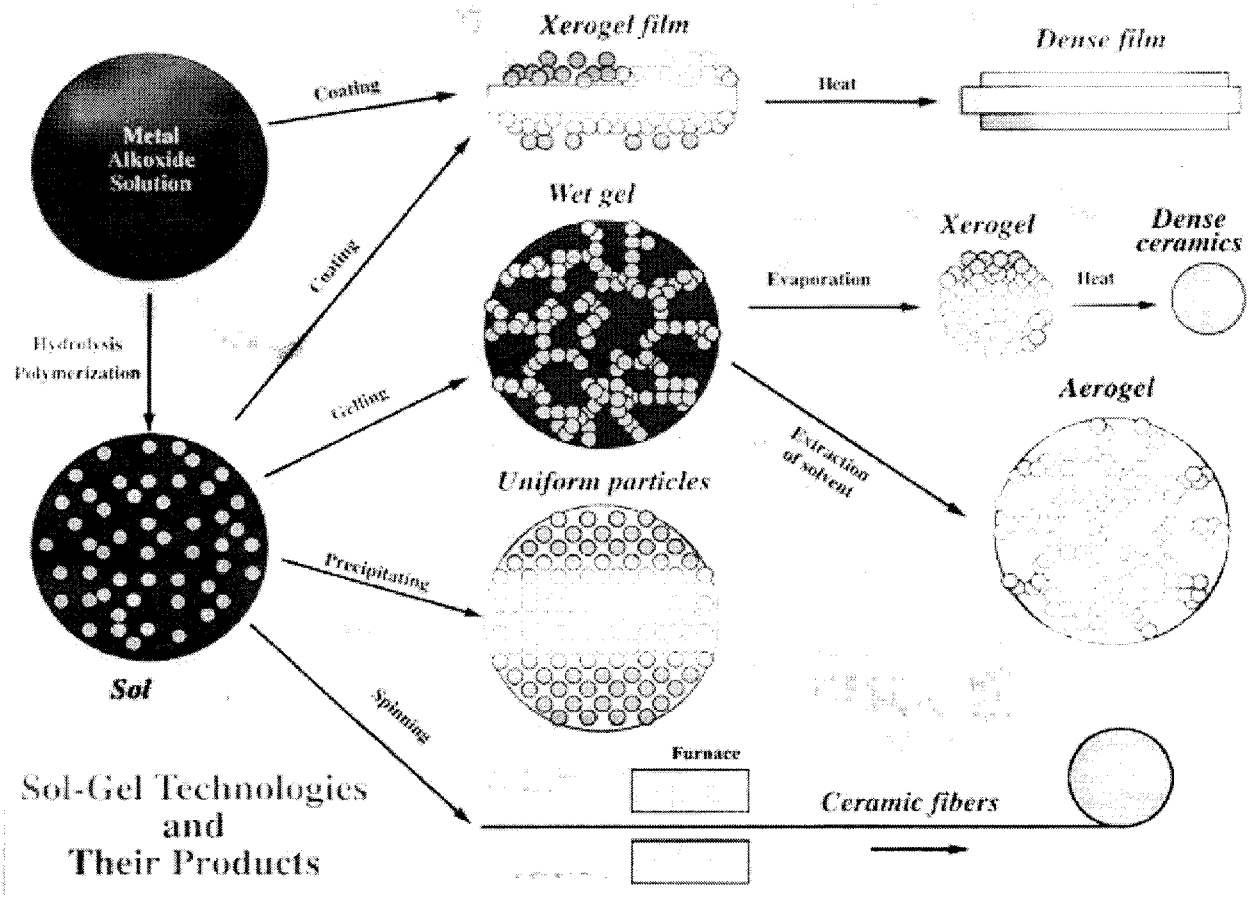


**Figure1.1** Schematic of a sol-gel processes and ceramic products.

The hydrolysis products (complex hydroxides) condense and form growing clusters through polymerization. The clusters join each other and as a result an interlocking

phase called "gel" is formed, which can be easily shaped. The sol-gel processing of ceramics offers a number of advantages over "traditional" powder processing of ceramics, such as increased purity and homogeneity (mixing occurs on the atomic level), reduced sintering temperatures due to small particle size, and ability to coat complex shapes. Disadvantages of sol-gel processing are high cost of raw materials, large shrinkage accompanying drying and sintering, and relatively long processing time for 3D objects [12].

Thin films produced through sol-gel processing overcome many of these intrinsic disadvantages of the technique. The early application of sol-gel coatings was in optical devices. Many new uses of sol-gel films have appeared in electronic components, protective films (e.g. corrosion and wear), membrane and sensor applications as well as biomaterials. Thin sol-gel films can be produced using small amount of raw materials, can be processed relatively quickly without cracking while large substrates can be easily accommodated. Therefore thin film coating has become one of the few commercial applications of the sol-gel technology [12].

### 1.3 Focus of the present study

Although many controlling parameters such as starting materials, aging time and heat treatment time and temperature in the sol-gel synthesis of hydroxyapatite have been investigated (reviewed in section 2.5) very few studies have addressed the effects of solvents on the HAp phase evolution and coating characteristics. In this work we are looking into the effects of organic solvents on a novel sol-gel system, which produces hydroxyapatite at relatively low temperatures (400-500°C). Employing different solvents in preparation of the solution affected the phase formation, purity, microstructure and morphology of the final sol-gel HAp product. The ability to control the microstructure and morphology of the resulting hydroxyapatite translates to a control of its bioactivity. The solutions made using different solvents also had different viscosity and surface tension, which affected HAp coating formation on metallic substrates. The knowledge obtained from this fundamental study was then applied to deposit HAp coatings on medical substrates such as titanium and medical grade

stainless steel wires. Coating of coronary stents with hydroxyapatite through this sol-gel process was also attempted.

# CHAPTER 2

# LITERATURE REVIEW

## 2.1 Biomaterials

Glasses and ceramics have been applied in the biomedical industry due to their compatibility with the biological environment and their resistance to environmental attack. The applications of ceramics include replacements for hip [13], knees [14], teeth [15], tendons and ligaments [16] and repair for periodontal disease [17], maxillofacial reconstruction [18], augmentation and stabilization of jaw bone [2], spinal fusion [19] and bone fillers after tumour surgery [2]. They have also been applied in dentistry and as a hard tissue replacement in musculo-skeletal systems such as bone and teeth, but their clinical success requires a good interface between the implant and the tissue and also a good match of mechanical properties at this interface [2].

Depending on the response an implant elicits in a living tissue different mechanisms of implant- tissue attachments have been categorized. According to I. Hench [2] these mechanisms can be summarized as follow:

1- Nearly inert dense biomaterials. In this category attachment occurs through the growth of the hard tissue into the irregularities of the surface by cementing the device into the tissue (morphological fixation). In this category of biomaterials the movement that occurs between the implant and the hard tissue usually leads to deterioration of the function of the implant. Alumina, both in the form of single and polycrystalline form, is in this group.

2- Porous inert implants. In this case the attachment is achieved by the ingrowth of the bone into the pores of the material (biological fixation). This ingrowth provides a larger area of attachment and consequently creates an increased resistance to movement. In order to keep the tissues in pores healthy, the pores should be 100-150μm in diameter to provide the tissues enough blood flow to survive. This requirement of the porous implant will lead to low mechanical strength and therefore limits the application of implants of this type to coatings and unloaded applications. Hydroxyapatite-coated porous metals can be considered in this category.

3- Dense, nonporous (porous) resorbable ceramic. In this case ceramic implant is designed to be slowly replaced by the bone. The criteria for this type of implants are first, to maintain the strength of the implant throughout the degradation process and second to control the degradation rate in order to match it with the rate of tissue replacement. Calcium sulfate and tricalcium phosphate are good candidates for resorbable biomaterials.

4- Dense nonporous materials with reactive surfaces. These implants will chemically bond to bone (resulting in bioactive fixation). The term bioactive is used for those categories of biomaterials, which "elicit a specific biological response at the interface of the material which results in the formation of a bond between the tissues and the material" [1]. Bioactive glasses, bioactive glass-ceramics and hydroxyapatite (HAp) are in this group of implants.

### 2.2 Calcium phosphate ceramics

Different phases of calcium phosphate ceramics are used in either resorbable or bioactive materials. A slight difference in composition can change a biomaterial from resorbable to bioactive or even inert [2].

The type of stable phases of calcium phosphate ceramics, depend on temperature and presence of water either during processing or while in use. Figure 2.1 shows the phase diagram for CaO and $P_2O_5$. As it can be seen HAp is the stable phase till 1360°C when water partial pressure is ~66 KPa, without water $C_4P$ and $C_3P$ are stable phases. As it can be seen in Fig. 2.1, by increasing the water pressure the temperature range of HAp stability increases [2].

Two phases of calcium phosphate materials are stable at the body temperature and in aqueous media. For pH < 4.2, $CaHPO_4.2H_2O$ (dicalcium phosphate, DCP) and for pH ≥4.2, $Ca_{10}$ $(PO_4)_6$ $(OH)_2$ (HAp) are the stable phases. At higher temperatures $Ca_3$ $(PO_4)_2$ (β-tricalcium phosphate, β-TCP) and $Ca_4P_2O_9$ (tetracalcium phosphate, TTCP) are stable. The high-temperature phases will interact with water or body fluids at 37°C to form HAp [2]. The reaction of formation of HAp on the surface of tricalcium phosphate (TCP) is proposed as follows [2]:

$$4\ Ca_3(PO_4)_2(s)+2H2O \rightarrow Ca_{10}(PO_4)_6(OH)_2(surface)+2Ca^{2+} + 2HPO_4^{2-} \quad (2.1)$$

According to the above reaction the solubility of TCP approaches the solubility of HAp. Micropores present in the sintered implants will increase the solubility of TCP as well as the increase in pH [2].

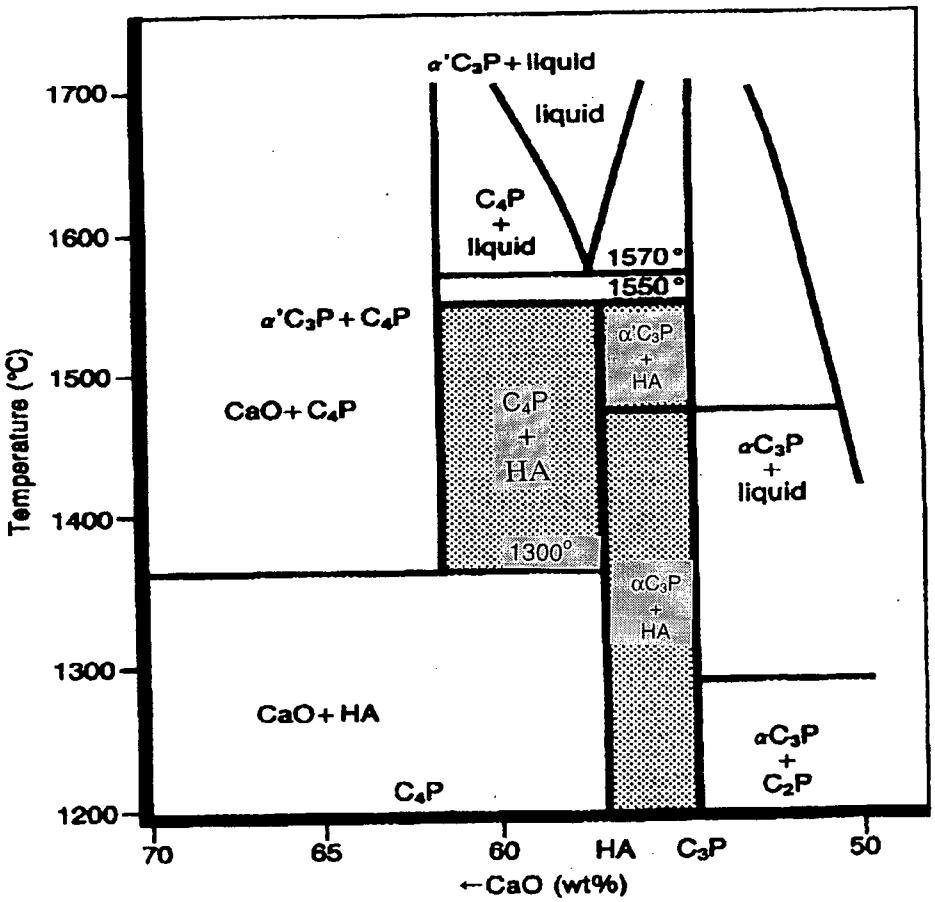


**Figure 2.1** Phase diagram of CaO and $P_2O_5$ binary system. From [2].

### 2.2.1 Mechanical properties

Mechanical properties of calcium phosphate ceramics are the main factor affecting their biomedical applications. The presence of porosity either in the form of micropores (<1μm) or macropores (>100μm) decreases both the compressive and tensile strength [2]. The following equations elaborate on this dependence:

$$\sigma_c=700 \exp(-5V_p) \quad (2.2)$$

$$\sigma_t = 220 \exp(-20V_m) \quad (2.3)$$

Where $\sigma_c$, $V_p$, $\sigma_t$ and $V_m$ are the compressive strength, total pore volume fraction ($V_p$=0-0.5), tensile strength and volume fraction of microporosity, respectively [2]. The compressive strength of dense HAp ceramics falls in the range of 120-900 MPa and the range for tensile strength is 38-300 MPa [6].

The low mechanical properties of calcium phosphate ceramics restricted their applications to (1) powders, (2) dental implants with reinforcing metal posts, (3) coatings, (4) small unloaded implants, (5) low loaded porous implants and (6) polymer-bioactive ceramic composites [20].

### 2.2.2 Bioresorption and biodegradation

Calcium phosphate (Ca-P) materials undergo a bioresorption and biodegradation process after being exposed to biological environment. "Biodegradation is the process caused by the action of living systems (e.g. microorganisims, cells) when material breaks down into its simpler components; reduces the complexity of a chemical compound or wears away by erosion" [20].

The Ca-P implant material undergoes both physical and chemical changes when introduced to the biological environment. Physical changes include disintegration, changes in micro and macroporosity of the implant and also change in the size and/or weight of the implant. Chemical changes primarily include reduction of pH in the implant environment thus changing its solubility. Consequently concentration of Ca and P ions increases in the implant microenvironment beyond the saturation level, resulting in deposition of a layer of Ca-P material on the surface of the implant or their incorporation into the new bone formed at implant/bone interface. Bioactivity of a material is defined as its ability to form a Ca-P compound on the implant surface when introduced to biological environment saturated with Ca and P ions, and therefore is related to the biodegradation of the material [20].

The Ca/P ratio of the starting precursor materials is an important factor in determining the Ca-P phases occurring in the final product, and thus affecting the solubility, biodegradation and finally bioactivity of the implant material. If the Ca/P ratio of the

starting material is less than 1.67 (i.e. the stoichiometric value for HAp), β-TCP forms along with HAp. If Ca/P ratio is higher than 1.67, the product will contain CaO along with HAp [20]. Although sintering temperature does not affect the β-TCP/HAp ratio of the final product, it changes the crystallinity of the phases, which will affect the biodegradation or biodissolution of the Ca-P materials. It is reasonable to believe that lower crystallinity will lead to higher dissolution rates [20].

According to LeGeros [20], the parameters affecting the solubility of Ca-P materials include (1) physical parameters (e.g. density), (2) composition, i.e. different composition and mixtures of Ca-P materials can greatly affect the extent and rate of the dissolution of the implant, (3) crystal structure and (4) crystallinity. The orders of relative solubility of some Ca-P compounds are as follows:

$$ACP \geq DCP > TTCP > \alpha\text{-}TCP > \beta\text{-}TCP \geq HAp$$

Where ACP is "amorphous calcium phosphate".

Bone cells will readily attach to Ca-P materials [20]. Cell proliferation and increased DNA synthesis were also observed due to increase in intracellular $Ca^{+2}$ ion concentration [21]. The increase in the concentration of calcium and phosphate ions resulting from dissolution of Ca-P materials also affects bone-cell activity [20]. One of the most important effects is the increased inhibition of bone resorption due to reduced osteoclast[1] formation and decreased activity of mature osteoclasts [20].

### 2.2.3 Mechanism of new bone formation

The dissolution of the Ca-P in acidic environments will lead to an increase in the concentration of calcium and phosphate ions in the surrounding solution. This will eventually lead to precipitation of apatite microcrystals, usually incorporating other ions such as $Mg^{2+}$, $CO_3^{2-}$, etc. along with the organic molecules. Other non-apatite Ca-P phases such as dicalcium phosphate dihydrate (DCPD) and octacalcium phosphate (OCP), which are more stable toward dissolution, may also hydrolyse to $CO_3$-containing apatite [20]. The series of events which will finally lead to the formation of

[1] Osteoclast: any of the large multinucleate cells closely associated with areas of bone resorption [22]

a biological bond between the implant and the bone can be presented as follows [20]: (1) biodegradation/bioresorption of bioactive material, (2) formation of adhesive proteins and collagen fibril due to the differentiation of osteoblast[2], (3) formation of $CO_3$-apatite microcrystals on the degrading Ca-P implant material, and (4) simultaneous mineralization of the collagen fibrils and incorporation of the new apatite crystals.

### 2.3 Calcium phosphate bone cements

Calcium phosphate bone cements are mixtures of various calcium phosphate powders, such as $CaHPO_4.2H_2O$, $Ca_4(PO_4)_2O$, $CaHPO_4$, $Ca_8H_2(PO_4)_6.5H_2O$, $Ca(H_2PO_4)_2.H_2O$, or TCP and water or another liquid ($H_3PO_4$ or $Na_2HPO_4$). The mixture transforms into HAp during setting, forming a porous body even at 37°C [6]. The process of dissolution-precipitation of Ca-P phases constitutes the setting process and imparts mechanical strength to the final product. The main advantages of calcium phosphate bone cements are their high biocompatibility, bioactivity and osteoconductivity, while their main disadvantage is their relatively poor mechanical strength. The wet compressive strength of calcium phosphate cements range from 21 MPa to 51 MPa, which is affected by factors such as powder-to-liquid ratio, and porosity of the cement [23]. Calcium phosphate bone cements are currently used as bone fillers, filling of the teeth root canal and as drug delivery systems [6].

### 2.4 Hydroxyapatite-based biomaterials

#### 2.4.1 HAp powders

There are several techniques to produce HAp powder, generally classified as wet methods and solid-state reactions. The wet methods can be divided into three groups: precipitation, hydrothermal technique, and hydrolysis of other calcium phosphates [6]. Depending on the technique, materials with various morphology, stoichiometry, and level of crystallinity can be obtained. There are also other alternative techniques for preparation of HAp powders, such as sol-gel, flux method [24], electrocrystallization

[2] Osteoblast: a bone-forming cell [22]

[25], spray pyrolysis [26], freeze-drying [27], microwave irradiation [28], mechano-chemical method [29], or emulsion processing [30].

### 2.4.2 Dense HAp ceramics

Dense HAp ceramics are obtained through shaping and pressureless sintering of HAp powders at moderately low temperatures (1000-1200°C). However, hot pressing (HP), hot isostatic pressing (HIP) or HIP-post-sintering makes it possible to decrease the densification temperature and grain size, and achieve higher densities. Unfortunately, due to poor mechanical properties, applications of HAp dense ceramics have been limited to low-loaded implants. Due to their good compatibility with human skin and tissues they are presently also used as devices for monitoring of blood pressure and blood sugar, or optical observation of inner body tissues [6].

### 2.4.3 Porous HAp ceramics

Porous HAp materials have been applied as bone substitutes as they show a strong bonding to the bone. Bone will grow into the pores providing mechanical interlocking and thus increasing the mechanical strength of the HAp implant/bone assembly. A minimum pore size of 100μm is necessary to enable the ingrowth of bone and blood supply to the bone. This large size of the pores will in turn decrease the mechanical properties of the implants. The traditional way to produce porous HAp ceramics is to mix the powder with a pore-creating agent, or cast the powder into $CaCO_3$ skeleton, which will be removed later by dissolution. There are some low temperature processing alternatives, including conversion of a porous skeleton of $CaCO_3$ into HAp under hydrothermal conditions. Porous HAp materials have been used in medical applications in the form of blocks or granules for filling bone defects, drug delivery systems, and alveolar ridge augmentation [6].

### 2.4.4 HAp-based ceramic composites

HAp ceramic composites attempt to address the problem of low mechanical reliability of pure HAp ceramics. Many reinforcements, including particles [31], whiskers [32], long fibers [33], partially stabilized zirconia particles [34], and metal dispersoids [35]

have been used in producing HAp composites. Although these may improve mechanical reliability of HAp ceramics, at the same time introduce new limitations such as lower biocompatibility, stress shielding of the hard tissue, carcinogenic effect especially when fibrous materials are used as reinforcements, and more complex and difficult processing. HAp/TCP ceramic composites have been also developed, not to improve mechanical properties but to affect biological performance, e.g. by controlling the biodegradation rate of the composite implant [6].

### 2.4.5 HAP/bioactive glass composites

Combination of bioactive glasses with HAp results in biomaterial with improved mechanical properties without degradation of biocompatibility or bioactivity [6]. In spite of high bioactivity, high biocompatibility and superior mechanical properties to HAp ceramics, HAp/bioactive glass composites are used as coatings or small, non-loaded implants, as their application has not been successful in hard tissue replacement.

### 2.4.6 HAp coatings

The concept of HAp coatings on the metal implants combines the mechanical advantages of metal and bioactive properties of HAp. The HAp coating prevents the encapsulation of bioinert metal implant with fibrous tissues, improves the integration of bone into the implant and provides a stronger bond between the implant and bone. HAp coating also decreases the release of metal ions from the implant into the physiological surrounding.

Different methods have been proposed to apply HAp coating on metallic implant, such as hot isostatic pressing [8,36], oxy-fuel combustion spraying [37], magnetron sputtering [38], flame spraying [37], ion beam deposition [9,39], chemical deposition under hydrothermal conditions [40], electrochemical deposition [11,41], pulsed laser deposition [42], and sol-gel process. In addition to all the methods mentioned, plasma-spraying [7] technique has become the most popular method to fabricate HAp coatings.

Thickness of HAp coatings can vary in a wide range, from fraction of micrometer for ion beam / sol gel techniques, to hundreds of micrometer for thermal spray techniques.

Increase in the thickness of the coating will generally decrease the amount of metal ions introduced to body from the implant and extend the coating resorption time (the resorption rate can be as much as 15-30 μm per year). Presence of porosity in the coating layer will improve bone ingrowth and thus bonding. Main problem regarding the HAp coatings is delamination of the coating due to fatigue or thermal coefficient mismatch at the metal/HAp interface. To increase bonding strength between metal and coating, buffer layers such as bioactive glass or $Ca_2SiO_4$ have been considered [6]. A layer of dense uniform HAp can also be deposited on the metal surface through a biomimetic process of soaking the implant in simulated body fluid at 37°C, but the growth rate is slow, in the range of several micrometers per day [6].

### 2.4.7 HAP/polymer composites

HAp/polymer composites improve reliability and decrease stiffness of the HAp biomaterials. HAp/polyethylene and HAp/polylactide composites have been studied in depth [43]. HAp/polyethylene composites have good mechanical properties such as high fracture toughness and a Young's Modulus close to that of the bone (1-8 GPa, depending on orientation). Unfortunately these composites are not biodegradable and also due to the presence of the bioinert polymer their ability to bond to bone is low. HAp/polylactide composites are both biodegradable and bioactive but there are several reports on their toxic effect in body. The new approach is to precipitate HAp crystals on collagen fibers to produce the composite [6]. In spite of poor mechanical properties, HAp/collagen composites exhibit superior osteoconduction (as compared to HAp or collagen alone) and controlled biodegradability, which makes them a good candidate for bone filling applications.

## 2.5 Sol-Gel HAp

### 2.5.1 The Sol-Gel process

Sol-gel is a process in which an inorganic structure evolves from a solution (sol) following a chemical multi-step pathway. A "sol" is a colloidal suspension of ~1-100nm large solid particles in a liquid. These particles are under strong influence of short-

range forces such as van der Waals and surface charges. Transition metal alkoxides, $M(OR)_x$ are widely used as molecular sol-gel precursors to glasses and ceramics. Due to the high electronegativity of the OR group, M is always in its highest oxidation state and therefore is susceptible to nucleophilic attack [12]. The alkoxide will therefore undergo a hydrolysis upon introducing to the solvent. The hydrolysis process consists of a nucleophilic attack in which a proton is transferred from the attacking molecule to the alkoxide or hydroxo-ligand.

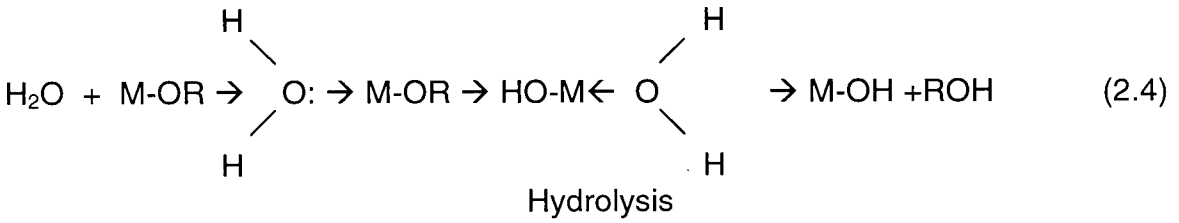


(2.4)

The protonated species will be then removed as either alcohol (alcoxolation) or water (oxolation):

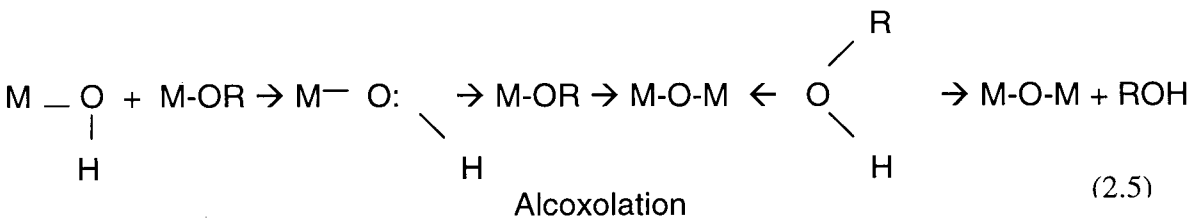


(2.5)

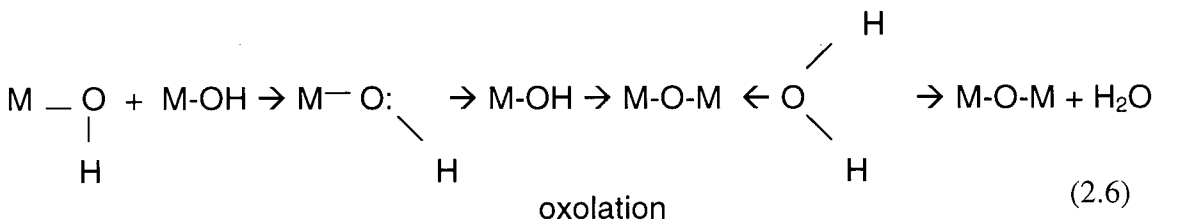


(2.6)

When the hydrolysis product is not yet saturated in coordination condensation can occur through olation:

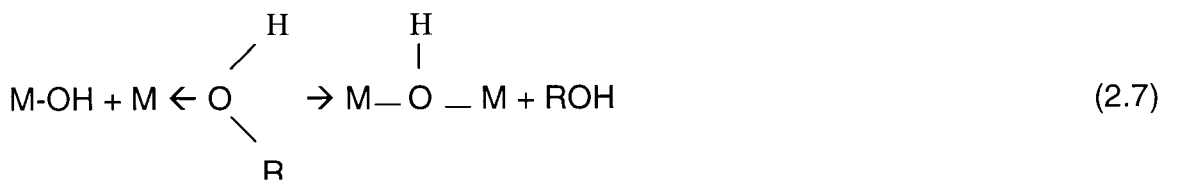


(2.7)

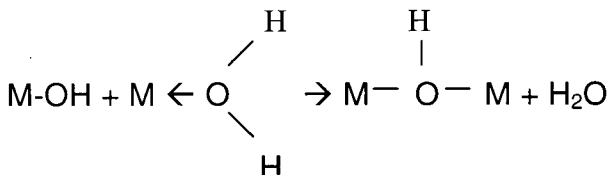

$$M\text{-}OH + M \leftarrow O(H)(H) \rightarrow M\text{—}O\text{—}M + H_2O \qquad (2.8)$$

The thermodynamics and kinetics of the hydrolysis, alcoxolation and oxolation are influenced by the nucleophilic strength of the attacking molecule, electrophilicity of the metal, charge stability of the leaving group, extent of coordination unsaturation of the core metal and molecular complexity of the metal alkoxide which is also dependent on the alkoxide ligand [12]. Catalysts are usually used to influence the rate of the hydrolysis and condensation process. For example, acid catalysts can protonate the negatively charged alkoxide groups thus enhancing the reaction kinetics [12]:

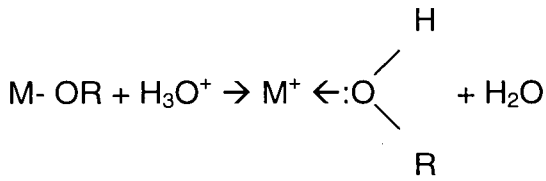

$$M\text{-}OR + H_3O^+ \rightarrow M^+ \leftarrow :O(H)(R) + H_2O \qquad (2.9)$$

The structure of the condensed products depends on the relative rate of the four reactions involved in the sol-gel: hydrolysis, oxolation, alcoxolation and olation. The extent of the contribution of each of these steps is also affected by parameters such as nature of the metal ion (M) and alkyl groups, molecular complexity, catalysts presence, concentration, type of solvent and temperature [12]. As a result of hydrolysis and condensation reactions inorganic polymers will form, and finally grow into clusters. The clusters then collide and link, leading to formation of a single giant cluster called the gel. At the time of gel formation many clusters are present although not attached to the spanning cluster. With time, the clusters would connect and as a result, the stiffness of the gel increases. The moment in which the last link is formed is called the gel point [12].

Following gelation, the steps of drying (solvent removal), calcinations (decomposition of hydrated oxide to oxide) and thermal consolidation (sintering) of the gel must be performed to produce a ceramic. At the first step of drying, the body would shrink due to removal of liquid from the gel pores through evaporation from the surface. As gel

pore size may be of nanometer range, surface tension strongly affects the drying process and may lead to gel cracking. While drying, the gel body becomes stiff and shrinks as the liquid recedes into the pores. Eventually liquid would be trapped inside the pores and evaporation continues by vapour diffusion through the body to the outside surface [12].

The calcinations and sintering of thus formed gels is performed in a single thermal treatment stage. Densification process is driven by the tendency of materials to reduce the interfacial surface energy between the solid and vapour by reduction of surface area. In case of gels due to enormous surface area of the complex porous structure (100-1000$m^2/g$), sintering can occur at exceptionally low temperatures [12], starting at several hundred degrees centigrade. For example, the HAp gels in this work were consolidated at 400-500°C.

The main advantages of sol gel over conventional methods of ceramic processing are as follows [44]:

1- High purity of starting materials
2- Homogeneity and excellent control of microstructure
3- Flexibility of shape in processing.
4- Low temperature formation and crystallization of the material, leading to lower cost and higher purity.

The disadvantages are [44]:

1- High cost of raw materials
2- Shrinkage/deformation due to solvent removal
3- Multiple processing step

### 2.5.2 Ceramic coatings by sol-gel

The most technologically important aspect of sol-gel processing is its ability to produce thin films prior to gelation. Comparing to conventional methods of coating such as chemical vapour deposition, evaporation, plasma spraying or sputtering, sol-gel film formation requires less, and low cost equipment. Sol-gel process has also the unique

ability to precisely control the microstructure of the thin film i.e. pore volume, pore size and surface area. Sol-gel thin films can be deposited on the surface of the substrate using the following techniques [12]:

1- Spin coating. The main advantage of this technique is its ability to produce a uniform thin layer. Spin coating process can be divided into the steps of deposition, spin-up, spin-off and evaporation, while evaporation accompanies other stages, Fig. 2.3. During the deposition an excess amount of sol is deposited on the surface, which will flow radially outwards at the start-up stage as a result of the centrifugal force. Droplets of excess liquids would leave the surface at the perimeters at the spin-off stage leaving behind a uniform, thin film [12].

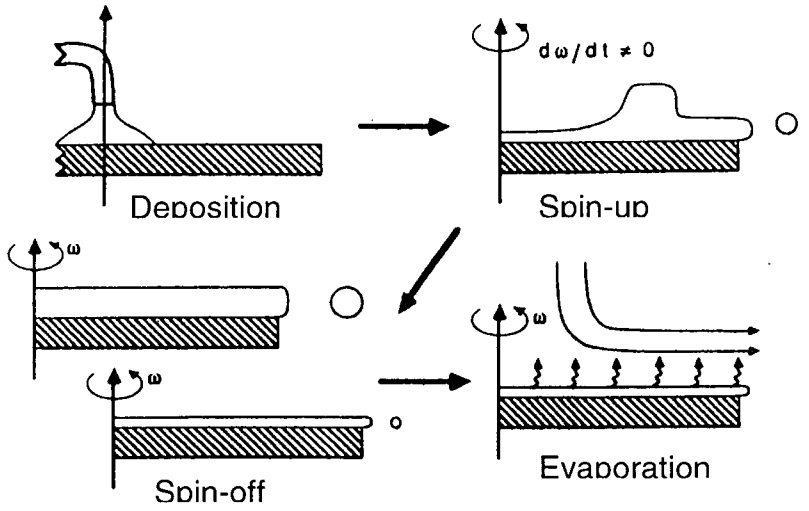


**Figure 2.3** Stages of the spin-coating process. From [12].

2- Dip Coating. Dip coating can be divided into five stages: immersion, start-up, deposition, drainage, and evaporation, Fig 2.2. In case of volatile solvents evaporation accompanies the start-up, deposition and drainage steps. Continuous dip coating is simpler as it eliminates the start-up and hides the drainage of the deposited film. A competition between six forces governs the film thickness: (1) viscous drag upward on

the liquid by the moving substrate, (2) force of gravity, (3) resultant force of surface tension in the concavely curved meniscus, (4) interfacial force of the boundary layer liquid arriving at the deposition region, (5) surface tension gradient, and (6) the disjoining or conjoining forces. The main advantage of dip coating is its ability to coat complexly shaped substrates [12].

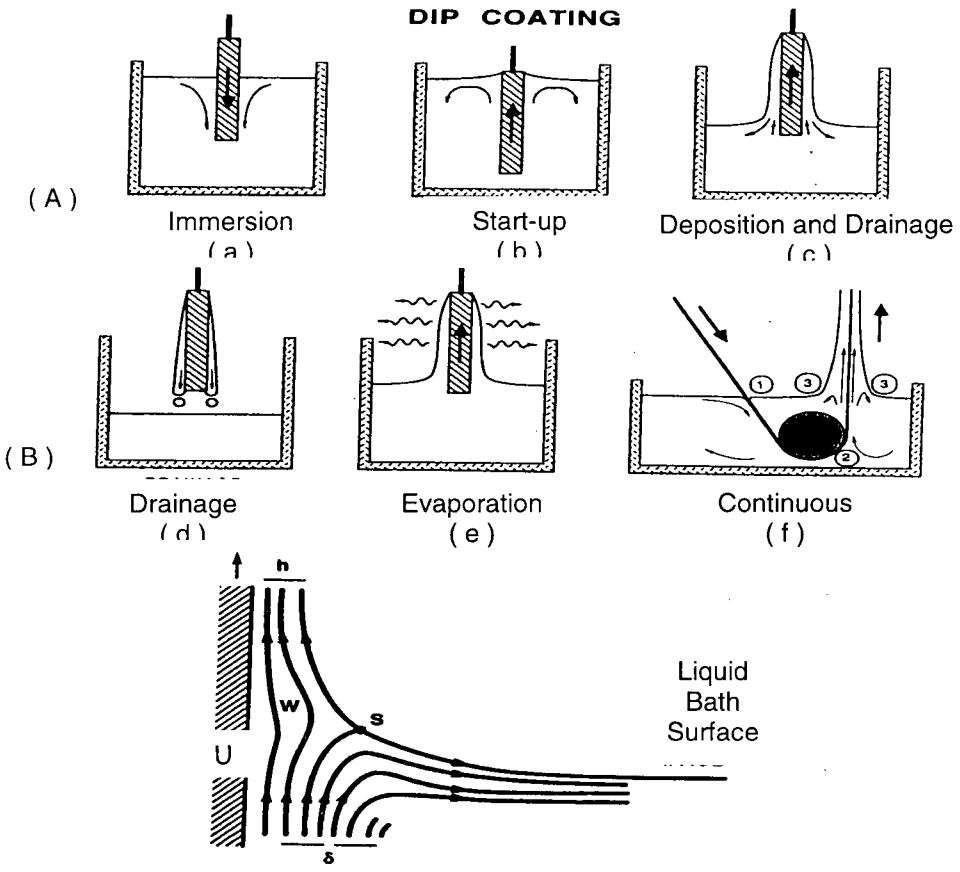


**Figure 2.2** (A) stages of dip coating process: (a-e) batch, (f) continuous. (B) Detail of the liquid flow patterns in area 3 of the continuous process. *U* is the withdrawal speed, *S* is the stagnation point, δ is the boundary layer, and, *h* is the thickness of the fluid film. From [12].

Other coating techniques applied to produce a thin film in sol-gel processing are:

3- Electrophoresis. In this method the conductive substrate is installed as an anode or cathode and the coating forms due to the deposition of charged particles mobilized due to an external current [12].

4- Settling: in which the particulate sols are deposited on the surface due to the force of gravity accompanied by the connective motion resulting from solvent evaporation [12].

### 2.5.3 Sol-gel HAp materials

Many studies have been conducted on the sol-gel synthesis of hydroxyapatite. Through these investigations different combinations of alkoxide precursors for calcium and phosphorous have been studied, which have resulted in a range of products with different hydrolysis and aging time, sintering temperature and a variety of by-products accompanying hydroxyapatite.

Jillavenkatesa et. al. [45] have used calcium acetate and triethyl phosphate as a source for calcium and phosphorous, respectively. They have applied X-ray diffractometry (XRD) and infrared spectroscopy (IR) as their main characterization methods. In this study they have also investigated the effect of organic solvents such as methanol, ethanol and propanol on their sol gel system. They have concluded that hydroxyapatite can be obtained in this system at temperatures as low as 500°C, though it is usually accompanied by calcium carbonates, which will decompose into calcium oxide at higher temperatures. They did not observe any significant effect induced by various organic solvents.

Layrolle et. al. [46] have produced amorphous calcium phosphate (ACP) through a sol-gel process, using calcium diethoxide and phosphoric acid as precursors and ethanol as solvent. They have shown that the ACP powder crystallizes to a carbonated hydroxyapatite and a trace of β-tricalcium phosphate before converting to pure hydroxyapatite at 900°C. They have also obtained a microporous structure through the decomposition of carbonated hydroxyapatite with the pore size of 0.2μm.

Y. Masuda et. al. [47], have used, calcium diethoxide and triethyl phosphite as starting metal alkoxide. They have investigated the effect of pH on the final phase formation of hydroxyapatite in their sol-gel system. They have been able to obtain pure, plate-like

hydroxyapatite using solutions with pH range of 6-8, water content of 60%, and calcining temperature above 600°C. It was shown that alkaline solutions with pH≥9 result in precipitates, which will turn into hydroxyapatite, calcium oxide and tri-calcium phosphate when calcined at 900°C. The acidic solid-free solution produces a single-phase hydroxyapatite when solidified and heated to 900°C.

Takahashi et. al. [48], have synthesized stoichiometric hydroxyapatite through a sol-gel route of calcium nitrate and phosphonoacetic acid in aqueous citric acid solution. A brown powder was obtained by heating the solution , which turned into hydroxyapatite after heating at 980°C for 7 hours. XRD experiment did not show any carbonate ions in the final hydroxyapatite.

G. Kordas et. al. [49], have investigated the feasibility of sol-gel process for the synthesis of hydroxyapatite. Calcium acetate and $PO(OC_2H_5)_3$ were used as precursors while methyl, ethyl and propyle alcohol were used as solvents. They investigated the evolution of the structure using X-ray diffraction, IR and FT-EPR. It was concluded that sol-gel method yields satisfactory results for HAp preparation. They have detected small amounts of CaO along with hydroxyapatite after heat treatment at 930°C, which can be removed upon washing with acetic acid and water. Using FT-EPR the authors have also showed that the network develops in one direction during hydrolysis and complexation. They have also mentioned that one-ethyl group remains unreacted after drying at 75°C.

J. Livage et. al. [50], have done a fundamental study on the sol-gel synthesis of phosphates, showing that polyphosphates cannot be synthesized under ambient conditions from $PO(OH)_3$ or $PO(OR)_3$. The hydrolysis of $PO(OH)_3$ is difficult while $PO(OR)_3$ leads to the formation of $[H_x(PO_4)]^{(3-x)-}$ species, which have high reactivity toward complexing and therefore do not condense. This effect will result in precipitation rather than gelation. They have also shown that dissolving $P_2O_5$ in alcohols results in $PO(OH)_{3-x}(OR)_x$ species, which have reactivities intermediate between $PO(OH)_3$ and $PO(OR)_3$ . According to their research Alkyl phosphates, $P(OR)_3$, are also suitable precursors in the sol-gel process of phosphates.

C. S. Chai et. al. [51] have shown that a critical aging of at least 24 hours is necessary to obtain pure hydroxyapatite. Shorter aging periods result in impure phases such as carbonates, which further decomposed to calcium oxide at 600°C. It is suggested that the solution should be aged till no abrupt weight loss is observed between 680°C and 750°C upon heating. It is concluded that the aging process is dependent on the calcium and phosphorous precursors (calcium diethoxide and triethyl phosphite in this research). Aging time increases with increase in the concentration of these reactants while it reduces with the reduction of solvent used in the sol-gel process. A compromise should be obtained with aging time and the amount of solvent used as it might adversely affect the chemistry and quality of the sol-gel HAp coating.

Jilavenkatesa et. al. [52] have conducted an electron microscopy study on the different stages of hydroxyapatite formation through a sol-gel process. Calcium acetate and triethyl phosphate have been used as calcium and phosphorous precursors. They have concluded that a nucleation-growth process controls formation of hydroxyapatite in this system. Increasing the temperature provides enough activation energy for crystallization. The fine structured matrix is believed to be of a calcium apatite nature as it is consumed by the crystallization and growth process. Hydroxyapatite crystals are observes to be equiaxial at temperatures below 1000°C. Higher temperatures induce hexagonal-shaped crystals, which is consistent with the hexagonal unit cell in which hydroxyapatite crystallizes.

Weng et. al. [53] have used calcium glycolate, phosphoric acid, and $P(OH)_x(OEt)_{3-x}$ as precursors while acetic acid was used as reagent to modify the calcium glycolate and also change the acidity of the mixture. They have been able to obtain a transparent gel depending on the amount of the acetic acid and the extent of stirring. They have attributed this behaviour to the large molecular size of the ethylene glycol solvent, which makes the reactions dependent on diffusion. They have also been able to synthesize calcium phosphates with different Ca/P ratios by changing the ratio of acetic acid/Ca.

Deptula et. al. [54] have produced spherical powders of hydroxyapatite with diameters of 100 μm using water extraction variant of the sol-gel process. The solution is prepared with calcium acetate and phosphoric acid as precursors. The solution is then

emulsified in dehydrated 2-ethyl-1-hexanol. Drops of the emulsion were solidified by extraction of water with this solvent. They have observed that the formation of hydroxyapatite starts above 400°C while formation of carbonated hydroxyapatite happens at 580°C.

Weng et. al. [55] have used an ethylene glycol solution of $Ca(OAC)_2.xH_2O$ and butanol solution of $P_2O_5$ as precursors for sol-gel hydroxyapatite. Acetic acid and ammonium nitrate were used as stabilizer and oxidizer, respectively. At 500°C poorly crystallized hydroxyapatite has been obtained through this process. They have been able to obtain well-crystallized HAp and a small amount of β-tricalcium phosphate when $NH_4NO_3$ was used as a stabilizer.

A new water based sol-gel process has recently been developed by Dean-Mo et. al. [56] at UBCeram. In this process calcium nitrate tetrahydrate and triethyl phosphite are used as starting precursors and water and ethanol as diluting media for the calcium precursor. They have observed the formation of HAp crystals at temperatures as low as 350°C. A more pure HAp phase has been developed in powders from ethanol based solutions while other calcium compounds such as tricalcium phosphate seemed to accompany HAp in merely aqueous-derived powders. In a follow up study, the effect of hydrolysis on this system has been investigated by the same group [57]. They have introduced a chemical pathway for hydrolysis reactions in this system. According to their speculations triethyl phosphite undergoes hydrolysis in the presence of water to form diethyl phosphorous esters:

$$P(OC_2H_5)_3 + H_2O \rightarrow HPO(OC_2H_5)_2 + C_2H_5OH \qquad (2.10)$$

Diethyl phosphorous ester may undergo further hydrolysis and as a result more OR groups will be replaced by OH group from aqueous environment:

$$HPO(OC_2H_5)_2 + H_2O \rightarrow HPO(OC_2H_5)_{2-x}(OH)_x + xC_2H_5OH \qquad (2.11)$$

The hydrolysed phosphates will further interact with Ca through a condensation polymerization reaction:

$$2HPO(OC_2H_5)_{2-x}(OH)_x + Ca^{++} \rightarrow [(OC_2H_5)_{2-x}O(H)P\text{-}O]_2Ca + 2H^+ \quad (2.12)$$

They have attributed the formation of TCP to condensation of hydrolysed phosphite molecules, which will further interact with calcium to form calcium phosphate derivatives [57]. The UBCeram group has also observed that the addition of acid catalyst will accelerate the rate of hydrolysis and condensation in this system. The work presented in this thesis originated from this process developed at UBCeram [56,57].

### 2.5.4 Sol-gel HAp coatings

HAp coatings on metallic implants combine good mechanical characteristics of metals with bioactive properties of hydroxyapatite. Many coating techniques have been developed to deposit a layer of calcium phosphate on metallic substrate. All these coating methods have the problem of a week mechanical bonding between the metal oxide layer and the calcium phosphate coating.

The sol gel process offers a relatively low coating temperature, results in stoichiometric and homogeneous coatings, and can yield both amorphous and crystalline films (this is important in order to control the film resorption process). The low temperature processing is an advantage when the heat treatment can adversely affect the properties of the substrate, such as phase transformation occurring in titanium at 883°C. Also, oxidation of metallic substrates at elevated process temperatures could be a problem. Spinning or dipping the sample in the solution results in thin sol-gel coatings. The films obtained with this method are usually thin (<1 μm) and therefore can easily undergo heat treatment process without cracking or substantial shrinkage, characteristic of the sol-gel method for bulk materials. It is also possible to uniformly coat both sides of planar and axially symmetric substrates such as pipes, rods, fibres and wires, not easily handled by more conventional coating methods.

Major processing stages involve producing a solution from suitable alkoxides or salts, hydrolysis and ageing of the solution, deposition of the coating, and heat treatment.

The heating process involves the removal of the organics and provides enough thermal energy for chemical and physical reactions necessary to form and densify hydroxyapatite. Many studies have been done on different starting materials, processing stages and characterization of hydroxyapatite thin films on different substrates, mainly titanium and stainless steel alloys.

Piveteau et. al. [58] have deposited a layer of mixed Ca-P and titanium oxide ($TiO_2$) on titanium substrate to improve the bonding between the substrate and the coating. A sol of titanium dioxide was mixed with a solution of calcium nitrate and phosphorous esters. The composite was then deposited on the surface of the titanium substrate, which has undergone various pre-heat treatments and has been blasted with aluminium balls to improve mechanical interlocking between the substrate and the coating. Spin coating was used to apply the solution on the substrates, which were then fired to 850°C. They have observed that the viscosity of the precursors and also surface topography of the substrate directly affected the surface topography of the coated samples. According to their results more viscous starting precursors produce rougher surfaces.

Haddow et. al. [59] have deposited a biphasic calcium phosphate (HAp and TCP) on quartz glass substrate through a sol-gel process. The coating has been deposited using dipping of the substrate in the solution and then firing the substrate to 1000°C. They have concluded that the coating thickness after firing at 900°C were significantly less that 1 μm for solution containing 1 M ethanol, with the thinnest coating being 0.15 μm thick. They have also observed that the time and atmosphere of heating affects the phases evolved in the coating, e.g. water molecule in the heating atmosphere will promote the formation of hydroxyapatite while in a dry atmosphere TCP and tetracalcium phosphate (TTCP) are more stable. It was reasoned that a biphasic calcium phosphate coating on a titanium substrate will increase the bioactivity of the coating as a more soluble Ca-P phase (TCP) along with an insoluble phase (HAp) will promote a rapid bone response.

Weng et. al. [60] have prepared hydroxyapatite coating on an alumina substrate using $Ca(NO_3)_2.4H_2O$ and $P_2O_5$ as starting precursors and ethanol as the diluting media. The coating showed good adhesion strength of about 10 MPa when fired to 500°C. They

have observed that increasing the temperature to 750°C will produce β-tricalcium phosphate as a by-product while it introduces more porosity to the morphology of the coating. Varying the processing conditions such as heat treatment time and temperature produced hydroxyapatite with various degrees of crystallinity and porosity.

A nanocrystalline layer of hydroxyapatite has been deposited through a sol-gel process on various substrates by Chai et. al. [61]. The solution was prepared using calcium diethoxide and triethylphosphite diluted in ethanol and then aged for seven days. The sol was then spin coated on various substrates such as Vycor glass, polycrystalline alumina, partially stabilized zirconia and single crystal MgO. Multiple layers of the coating were deposited with the prefiring temperature of 500°C and then 1000°C as the final treatment. The coating thus prepared was crystalline with the crystal size of 200-800 nm. They have also observed good coating/substrate adhesion. As it could be expected the relatively high firing temperature has produced calcium oxide as a by-product.

A hydroxyapatite thin layer has been coated on the surface of a single crystal Si (001) substrate through a sol-gel process by Hwang et. al. [62]. They have used phosphoric acid and calcium nitrate as phosphorous and calcium precursors, respectively. The solution has been spin coated on the surface, prefired at 300°C and then heat treated at 500°C and 700°C. The authors observed the formation of hydroxyapatite structure at 500°C while the formation of β-tricalcium phosphate started at 700°C. They have attributed the formation of β-tricalcium phosphate to the decomposition of carbonated hydroxyapatite during the final heat treatment at 700°C.

Gross et. al. [63] have investigated the changes occurring in the sol during the aging period and also the behaviour of the xerogels[3] upon heat treatment using $^{31}P$ nuclear magnetic resonance spectroscopy and thermal gravimetric analysis. The solution was prepared with calcium diethoxide and triethylphosphite as starting precursors. The solution was then aged for 24 hours and spin coated on the surface of titanium coupons and finally fired to 800°C. According to their experimental results, hydroxyapatite crystallization starts at 550°C and further heat treatment will remove the organic residues. The authors have also concluded that a minimum of 24 hours of

[3] Xerogel: dried gel, when drying has taken place in ambient conditions [12]

aging period is necessary to obtain pure hydroxyapatite, otherwise calcium oxide will be present as an impurity phase. According to their findings during the aging period the two alkoxide will react to form calcium and phosphorous diethoxide (OEt-Ca-O-$P(OEt)_2$), which will then condense to form $[Ca\text{-}O\text{-}PO_3]_n$ through a rapid reversible process.

Hwang et. al. [64] have coated porous alumina substrate with hydroxyapatite through sol-gel process. Their process uses calcium nitrate tetrahydrate and phosphoric acid as the starting precursors. The coated substrate was subjected to a heat treatment of 700°C. They have observed a shift in the peak positions of hydroxyapatite, which was attributed to the incorporation of residual carbon into the structure of hydroxyapatite.

Lopatin et. al. [65] have looked at the effect of drying and firing stages in a hydroxyapatite sol-gel using N-butyl acid phosphate and calcium nitrate tetrahydrate as precursors. Increasing the drying temperature suppressed the formation of hydroxyapatite. The authors have attributed this effect to the difficult rearrangements of M-O-M links formed during the drying stage. According to their hypothesis increasing the drying temperature will result in higher number of M-O-M bonds. It was also observed that hydroxyapatite crystallizes from a medium, consisting of hydroxyapatite nuclei and an amorphous matrix of organic compounds. Longer soaking time during drying will promote nucleation of hydroxyapatite crystals and therefore will lead to lower HAp formation temperatures.

Many of the results from the studies summarized above are similar regardless of the starting materials and the sol-gel process features. A critical aging period (24 hours according to most of the authors) seems to be necessary in order to obtain monophasic hydroxyapatite. In the case of insufficient aging, calcium oxide would be the impurity phase accompanying HAp. Formation of calcium oxide has been attributed to the unreacted calcium precursor, which will further react with water to form calcium hydroxide. The calcium hydroxide thus formed, will react with $CO_2$ (a by-product of decomposition of organic compounds) to form calcium carbonate, which will finally decompose to calcium oxide and $CO_2$. β-tricalcium phosphate is also observed to be present along with hydroxyapatite at higher processing temperatures (>600°C). This effect has been attributed to decomposition of the carbonated hydroxyapatite.

Carbonated hydroxyapatite forms due to incorporation of carbon into the structure of hydroxyapatite. This effect has been verified by a slight shift in the position of hydroxyapatite characteristic XRD peaks [64]. Many authors have observed that hydroxyapatite crystallizes from an amorphous Ca-P matrix so the crystal growth of the final HAp would depend on the decomposition rate of this amorphous phase. Due to the complexity of the chemistry involved in sol-gel processing of HAp no clear pathways for different stages of this process has been suggested as yet.

### 2.6 Stents

A stent is "a short narrow metal or plastic tube that is inserted into the lumen of an anatomical vessel (as an artery or a bile duct) especially to keep a formerly blocked passageway open" [22]. An English dentist, Charles T. Stent, who lived from 1807 to 1885, first used a stent. The first dental stent was described as "a new dental impression material of wax and gutta percha, a latex relative consisting of the milky sap from the Palaquium gutta tree in south-eastern Asia" [66]. During the First World War J. F. Esser of Holland used the dental stent as a urologic tool, which marked the first application of the dental impression in medical surgery [66].

The new technologies of the $20^{th}$ century such as discovery of antibiotics and biocompatible materials have provided the platform for the application of stents in endovascular operations. The new stents are wire mesh tubes commonly made of a medical grade stainless steel 316L, L indicating the low carbon content (0.03%). This alloy is composed of iron (60% to 65%), chromium (17% to 18%) and nickel (12% to 14%). Stainless steel provides good mechanical, chemical and physical properties but its biocompatibility remains an issue. Nickel (~55%)-titanium (~45%) (Nitinol) stents may also be used as they offer some better early biocompatibility although concerns regarding nickel leakage have limited their application. Tantalum is another option for materials used as stent material. Nitinol stents offer better radio-opacity, biocompatibility and mechanical properties although its clinical superiority to stainless steel stents has not been yet proved [67].

Stents are widely used to keep the blood vessel open following a balloon angioplasty. During this procedure the stent is placed on a balloon and manoeuvred into blocked

area. After the balloon is inflated, stent will lock in its place and will hold the artery open. Upon introducing to the blood vessel, stents permanently stay in the vessel and cannot be removed. Figure 2.4 shows the schematic picture of a stent placed inside the artery.

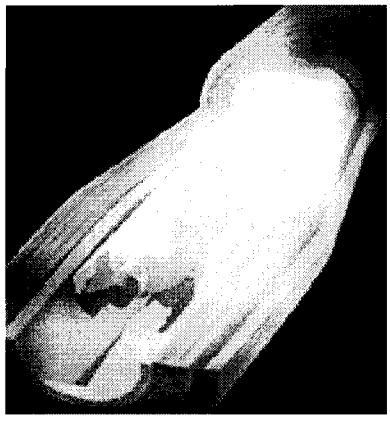

**Figure 2.4** Stent Placed inside the artery.

Restenosis[4], thrombosis[5], inflammation and neointima[6] formation are the early biocompatibility problems regarding stent implantation in the coronary arteries [69]. Although the mechanism of restenosis is not yet clear, it is believed to be the result of hyperproliferation of vascular smooth muscle cells which will finally lead to scar formation inside the blood vessel and therefore blocking the blood flow [70]. Late problems with the stents can be divided into two broad categories: mechanical failure due to material fatigue under the stress of cardiac contractions and chemical corrosion leading to the leakage of toxic substances, degradation products or contaminants [67]. The materials used as stents must have certain physical, chemical and mechanical properties. An expandable metal stents should have enough plasticity to retain the required size after expansion. On the other hand self-expanding stents should posses enough elasticity so that they can be compressed and then expanded while

[4] Restenosis: the re-occlusion of the vessels [68]
[5] Thrombosis: the formation or presence of a blood clot within a blood vessel [22]
[6] Intima: the innermost coat of an organ (as a blood vessel) consisting usually of an endothelial layer backed by connective tissue and elastic tissue [22]

maintaining sufficient radial loop strength. Corrosion resistance is the most important chemical characteristic regarding stents. The oxide layer formed on the surface of the metallic stent will retard corrosion and thus provide the metal with highly passive surface [67].

Multidisciplinary studies are now being conducted on stent research and as a result, new designs and different materials and coatings are being studied in order to enhance the quality of these prostheses. Experimental data suggests that the stent design and surface properties will strongly influence its performance [67]. In order to evaluate the effect of the coating on the performance of the stent several different coating materials have been studied. The results of these studies can be summarized as follows:

1- Nonbiodegradable synthetic polymers. Many polymer materials such as polyurethane, siloxane (silicon), polyethylene terephtalate, and cross-linked phosphorycholine have been coated on the surface of different stents. The tissue response, such as inflammation, neointima formation and thrombosis were then studied after implantation the stents in the animal model [71,72,73,74]. The experimental results of these experiments do not provide any final conclusion whether any polymer coating may improve the stents' biocompatibility, as the results vary from no apparent difference between the coated sample with the bare stent [74] to intense inflammatory responses in the presence of the coating [71] or better biocompatibility due to the coated surface [73]. However, polymers such as polyethylene and phosphorycholine seem to be suitable candidates for drug delivery systems on stent surface, in order to pharmacologically address the negative response of the tissue to stent presence [67].

2- Biodegradable synthetic polymers. Occlusion and a wide inflammatory response were observed upon implantation of polyglycoli/polylactic acid copolymer, polycaprolactone, polyhydroxy-butyrate/valerate copolymer (PHBV), polyorthoester, polyethyleneoxide/polybuthlene terephtalate copolymer (PEO/PBTP), and low molecular weight poly-l-lactic acid (LMWPLLA) coated stents [71, 75]. High molecular weight poly-l-lactic acid (HMWPLLA) coatings show no evidence of chronic inflammation. Among biodegradable polymer coatings PLLA is also regarded as a good matrix for temporary drug release.

3- Natural coated stents. In this case the surface of the stent (either bare or pre coated) is encased with fibrin [67]. Theoretically the natural coating should minimize inflammation and other negative tissue responses. A significant reduction in platelet deposition has been indeed observed by Baker et. al. [76] after implantation of a titanium self-expandable stent coated with fibrin and impregnated with Heparin. Stefanid et. al. [77] have covered the conventional stent with autologous vein or artificial graft which has produced significantly enhanced results but the process is yet too complex to be widely adopted.

4- Heparin coated stents. Heparin[7] coatings have shown to be effective in the reduction of thrombosis but their effect on the neointima formation needs to be established [67].

5- Drug-eluting stents. Much interest has been focused on loading a drug onto a stent to limit the early thrombogenicity and late neointima formation. Drugs maybe released by diffusion mechanisms or during polymer break down [67].

6- Polymeric stents. Polymeric stents have been developed using Dacron [78], polyglycolic acid [79], and biodegradable stent in collagen [79]. These stents are applied through angioplasty, which will then degrade inside the vein. The efforts to develop biodegradable stents have recently slowed down due to the complexity of the process and also acceptable performance of the metallic stents, while the idea of a biodegradable stent loaded with drug is still quite appealing [67].

7- Radioactive stents. Certain amount of radioactive doses delivered at the site of stent implantation may decrease the negative responses of the tissue. Radioactivity can be produced by either particle bombardment or ion implantation of the metallic surface, which on the other hand may affect the corrosion properties of the surface. Delivering radioactive isotopes through an eluting system can be another alternative [67].

To enhance the effectiveness of stents and broaden their applications to more complex lesions, better biocompatibility needs to be achieved. The new generation of stents should be less thrombogenic coronary endoprostheses and more tolerable by the body

[7] Heparin: a mucopolysaccharide sulfuric acid ester that is found specially in liver, that prolongs the clotting time of blood [22]

environment. This provides the rationale for studying the possibility of HAp coatings on stents, as presented in this thesis.

# CHAPTER 3
# SCOPE AND OBJECTIVES

## 3.1 Scope of investigation

Ceramics have been used in medical applications due to their biocompatibility while ceramics like hydroxyapatite and bioglass® have bioactive characteristics in addition to their compatibility with body environment. Although low mechanical strength of bulk bioceramics has limited their application in areas where mechanical durability is critical, they are still used in forms of composites or as coatings on a wide range of prostheses. Bioceramic coating provides enough biocompatibility and bioactivity for the implant which otherwise would be biologically inert or even elicit negative response in the surrounding tissues.

Sol-gel process allows fabrication of thin film ceramic coatings on various substrates. The main advantages of this simple processing method are the homogeneity of the final coating, control of its microstructure, ability to produce thin films (<1μm), and low temperature of heat treatment. The low temperature factor is of great importance in biomedical applications as the processing temperature of the coating might adversely affect the mechanical properties of the substrate. Thus, sol-gel synthesis of hydroxyapatite has been studied in the present thesis. The resulting coatings should have good adhesion to the substrate such that they are not damaged (or removed) during surgical implantation. In the case of stents, the application considered in this thesis, the coatings should resist delamination upon expansion of the stent in the arteries. Crystallization of the coating also needs to be controlled as it will further affect the rate of dissolution of the thin film into the blood stream while affecting the plasticity of the coating.

In order to produce a high quality HAp coating through a sol-gel system comprehensive understanding of the particular system as well as sol-gel technique in general seems necessary. Understanding the effect of controlling parameters in the sol-gel process, such as solvents and heat treatment temperatures, provides valuable knowledge to fulfill specific qualifications necessary for an individual application. In this respect, the scope of this work is to study the effect of organic solvents on the phase

evolution of hydroxyapatite in a novel, relatively low temperature sol-gel process. Very few previous studies have addressed the effect of the solvents on HAp sol-gel systems. The knowledge gained through this fundamental study is then applied to develop an optimum coating process for titanium substrates (flat) as well as stainless steel coronary stents (~0.1mm thin wires). The latter is the first attempt to apply hydroxyapatite as a biocompatible coating on such implants. Several characterization techniques such as SEM, XRD, and IR spectroscopy are used in order to evaluate the obtained coatings.

### 3.2 Objectives

The general objective is to investigate the effects of organic solvents (methanol, ethanol, propanol), on the phase evolution of hydroxyapatite in triethyl phosphite-calcium nitrate sol-gel system. The study objectives can be broken down as follows:

1- Characterize the phases present in the heat-treated HAp powders at various temperatures to monitor phase evolutions, and crystallization.

2- Investigate the effect of organic solvents on the morphology of the sol-gel HAp powder.

3- Investigate properties of HAp coatings from sols obtained using various solvents.

4- Apply and characterize the HAp sol-gel coatings on different model metallic substrates to optimized process parameters.

5- Apply and characterize the optimum HAp sol-gel coatings on commercial coronary stents.

These investigations were carried out using the following techniques:

1- Phase identification of the dry and sintered powders was carried out by qualitative X-ray diffraction (XRD).

2- Thermal gravimetric analysis (TGA) and differential thermal analysis (DTA) were used to investigate thermal behaviour of the dry gels upon heating.

3- Scanning electron microscopy (SEM) was used to observe powder morphology and also coated surfaces. Electron dispersive spectrometry is used in order to study the elemental composition of the surface of coated and uncoated substrates.

4- Solid-state infrared (IR) analysis is carried out to characterize the coatings, obtained from different solvent systems, on the model titanium substrates.

# CHAPTER 4

# EXPERIMENTAL METHODOLOGY

The sol-gel precursors consist of triethyl phosphite and calcium nitrate tetrahydrate, dissolved in organic solvent, i.e. methanol, ethanol, or propanol. Powder processing, characterization, and coating processing and characterization follow the sol preparation. Therefore, this experimental and methodology chapter is divided into three sections: (1) general procedures, (2) sol-gel powder preparation and characterization, and (3) sol-gel coating preparation and characterization. Sample preparation procedures for characterization experiments and instrumental information are also included. The second section of this chapter describes the preparation and heat treatment of sol-gel hydroxyapatite powder. Characterization processes of the sol-gel powder are also provided. In this section phase evolution upon heat treatment, and microstructure of the sol-gel powders are investigated. The third section details the coating and characterization procedures for the HAp coatings on various substrates. Coating procedures usually follow the sequence of (a) substrate surface treatment (preparation); (b) coating, (c) heat treatment, and (d) characterization. The samples were characterized using X-ray diffractometry, FTIR spectroscopy, scanning electron microscopy, and energy dispersive spectrograph.

## 4.1 General procedures

### 4.1.1 Materials

Unless otherwise stated, all materials were used as received. Triethyl phosphite ($P(OEt)_3$) and calcium nitrate tetrahydrate ($Ca(NO_3)_2 \cdot 4H_2O$) were obtained from Fisher Scientific and Aldrich, respectively. Sodium carbonate and Borax were used as neutralizing agents for acid treated stainless steel wires and were obtained from Fisher scientific and Greenbarn Potters Supply, respectively. Titanium substrates had a thickness of 0.127mm and were manufactured by Alfa Aesar. Medical grade stainless steel (316L) wires and coronary stents were provided by MIVI technologies of Vancouver, BC, and were used as coating substrates.

### 4.1.2 Analysis

Thermal gravimetric analysis was conducted on powder samples obtained from solution prepared from different organic solvents using a Perkin Elmer, 7 series, Thermal Analysis System, in order to monitor the weight loss of the powder upon heating. The tests were done at a heating rate of 10°C/min, from ambient to 1200°C. These experiments were conducted at the Institute of Materials Science and Manufacturing, Chinese Culture University, Yang Ming Shan, Taipei , Taiwan, our collaborators on this project.

Phase identification of calcined powder and thin film coatings was done using X-ray diffractometer Rigaku Rotaflex 200, Tokyo, Japan, using CuKα (1.54 nm) with 2θ of 25-40° with the step size of 5°/min. Powder samples were packed in an aluminium sample holder and then exposed to radiation. To investigate thin coatings, and especially coatings on wires and stents, powders were obtained from the coating solution, following the same process as for the coatings. The powder was then ground with a small amount of ethanol and applied as a thin layer on a glass substrate. The thin layer on the glass substrate was then dried and heat-treated along with the actual coated substrates to simulate the coating heat treatment conditions. After heat treatment, the glass substrates were directly subjected to further XRD tests.

Scanning electron microscopy was conducted for microstructural examination, using a Hitachi SEM. Due to the small size of the coated samples and dry gels, they could be easily placed on the stub and be examined. Except for the bare metallic substrates, all the samples were gold coated prior to SEM examination. Energy dispersive X-ray analysis was carried out to investigate the elemental composition of the surface of coated substrates.

Infrared spectroscopy was carried out using a Perkin Elmer system 2000 FTIR. Solid-state analysis was conducted on coated samples using KBr as background.

## 4.2 Powder preparation and characterization

Figure 4.1 schematically shows the so-gel HAp synthesis procedure. Phosphorous sol was prepared by hydrolysing small amount of triethyl phosphite (5.08 g), with distilled water (the molar ratio of phosphite/water was kept at 3) under vigorous stirring, with

the use of nitric acid as a catalyst. A 2.1N acid solution (10.2 g) was first added to the phosphorous alkoxide, aged for 5 minutes, and followed by the addition of a second solution. The second solution was prepared by dissolving calcium nitrate (11.80 g) into either one of three organic solvents (25 ml of methanol, ethanol or 1-propanol). The mixture was then stirred for 30 minutes followed by an aging period of 24 hours. The aged sol was then oven dried for 24 hours at 80°C until a white, dried gel was obtained. This procedure was first proposed by Dean-Mo et. al. [56].

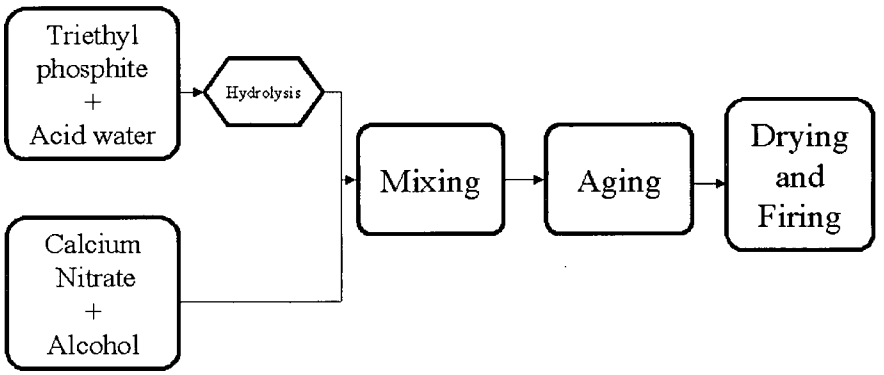


**Figure 4.1** Flow chart of so-gel HAp synthesis procedure.

The dry gel was ground and heat-treated at different temperatures (375, 425, 445, 465, 500 and 545°C). The heat treatment temperatures were chosen based on DTA results, to monitor phase evolution in the gel upon heat treatment. Powder samples were placed in the furnace in alumina crucibles. The temperature was then increased to the desired level, at which the sample was instantly removed from the furnace. XRD and SEM tests followed heat treatment procedure to investigate the phase composition and morphology of the calcined powder.

## 4.3 Coating preparation and characterization

### 4.3.1 Titanium substrates

In order to obtain a good adhesion between the coating and substrate, and also to increase the wetting of the substrate by the solution, the surface of the substrate should be roughened. This can be accomplished either through a chemical treatment, in which the substrate is exposed to a corroding environment, e.g. strong acid, or mechanical roughening such as SiC ball blasting or sand blasting. Mechanical methods of surface roughening tend to be more destructive and are not suitable for substrates with complex shapes, concave surfaces, or fine structures such as wires. In this work titanium substrates were chemically treated (i.e. partially corroded) in phosphoric acid (85%) at 50-60°C for 30 minutes. A number of titanium substrates were also subjected to sandblasting prior to coating.

Pre-treated titanium substrates were spin coated with the sol-gel hydroxyapatite precursor solution, prepared using different organic solvents as diluting media as described above. The spin coating was carried out using a commercial spin coater (Headway research Inc. EC101) with the speed of 3000 rpm for 20 seconds. IR spectroscopy, SEM, and EDS tests were done on the coated surfaces to investigate the chemical composition and surface morphology of the coating layer. Coated samples were then placed in simulated body fluid (SBF) for a period of seven days after which they were removed and rinsed with distilled water and air dried for three days. The SBF composition is presented in appendix I. Formation of apatite crystals on the surface of the coating, which is an indication of the bioactivity of the coating [80], was investigated with SEM.

### 4.3.2 Stainless steel substrates

#### 4.3.2.a Wires

It is believed that a rough surface improves the adhesion of ceramic coatings to metallic substrates, e.g. stainless steel substrate, as the adhesion is mainly governed by mechanical interlocking [81]. In order to find the best chemical treatment for the wire's surface and produce a sufficient degree of roughness on the surface, the effect of phosphoric acid (85%), nitric acid (70%), and hydrochloric acid (37%) on the

stainless steel wires was tested. The acid solutions were diluted in water by of 50 vol% (equivalent to 8 N for the phosphoric acid, 20 N for the nitric acid, and 86 N for the hydrochloric acid) . The stainless steel wires were exposed to the acidic solutions for 30 minutes at 70°C. The wires were then neutralized in an aqueous solution of 1.3 g/l $Na_2CO_3$ and 0.4 g/l Borax ($Na_2B_4O_7$) at 70°C for 4 minutes following a process proposed by shieu et. al. [81]. To investigate the effect of exposure time on the extent of etching, stainless steel wires were etched in 2.4N HCl solution for 10, 20, 30, 40, 50, and 60 minutes. The samples were then neutralized and studied using SEM.

The surface treated wires were shaped (bent) to resemble the shape of an actual stent and dip coated using an in-house made dip coater, with dipping rate of 14 cm/min. The coating solutions were the hydroxyapatite sols prepared using water, methanol, ethanol and propanol as diluting media for calcium nitrate, as described above. To investigate the effect of the solution concentration on the coating properties, methanol and ethanol sols were also prepared with a dilute concentration of calcium nitrate in the organic solvent by increasing the amount of the solvent to 50 ml (1M), while Ca/P ratio was kept at 1.67 (hereafter referred to as 1M solution).

The coated wires were dried at 80°C and fired at 500°C in air. SEM was used to investigate the surface of the wires after coating. In order to qualitatively study the effect of stress on the coating integrity, such as microcracking or de-bonding of the coating from the surface, the wires were bent back after the heat treatment. The unbending simulated the deformation of real stents during placement in blood vessel. The surface morphology of coatings fired at 500°C for different time periods (10, 20, 30, 40, 50, and 60 minutes) was studied using SEM. To investigate the effect of the firing time on the coatings, XRD was done on thin layers of powder heat treated on glass substrates at 500°C for various time periods (10, 30, and 60 minutes).

#### 4.3.2.b Stents

Stents obtained from two different stages of preparation (de-oxidizing and electropolishing) were coated and studied in this section.

As-received de-oxidized coronary stents were coated with HAp solution (1M) using a dip coater with withdrawal speed of 14 cm/min. Coated de-oxidized stents were then

heat treated at 500°C for 10 minutes and studied under SEM. Stents were then inflated using a commercial rapid exchange catheter with a semi-compliant balloon. The effect of stent deformation on the coating quality was investigated with SEM.

Electropolished stents were surface treated using a 2.4N hydrochloric acid aqueous solution at 70°C for 10 minutes and were neutralized following the same procedure as for the stainless steel wires. Samples were then coated with methanol-based sol prepared using 1M calcium nitrate solution, and a dip coater with a withdrawal speed of 14 cm/min. Stents were manually shaken after dip coating in order to remove the extra solution droplets on the surface, dried at 80°C and fired at 500°C for a period of 10 minutes. The coatings were studied under SEM.

# CHAPTER 5

# EXPERIMENTAL RESULTS AND DISCUSSION

## 5.1 Phase evolution in sol-gel hydroxyapatite

### 5.1.1 Results

#### 5.1.1.a X-ray diffraction

Figures 5.1, 5.2 and 5.3 show the XRD patterns of calcined sol-gel hydroxyapatite (SG-HAp) powders derived from methanol, ethanol and propanol based gels, respectively, heat treated at different temperatures. The methanol-based sample, calcined at 375°C (Figure 5.1), consists of a mixture of calcium phosphates $Ca_3(PO_4)_2$ (TCP) and $Ca_2P_2O_7$ (PP), and calcium carbonate. At 425°C small peaks appear at $2\theta \cong 37.5^\circ$ and $2\theta \cong 41.2^\circ$, characteristic of calcium oxide and calcium nitrate, respectively. At 445°C, a well-crystallized calcium nitrate is present along with TCP and $Ca_2P_2O_7$. Broad HAp peaks also start to appear, at $2\theta$ between 31° and 33° (reference: diffraction pattern JCPDC #9-432 (presented in appendix II)). At 460°C amount of amorphous[8] HAp increases, while calcium nitrate peaks start losing their intensity due to its decomposition to calcium oxide and nitrogen dioxide. At 500°C, a well-crystallized hydroxyapatite is present together with TCP and a small amount of $Ca_2P_2O_7$. The reflection intensity of HAp peaks has grown at the expense of the TCP, $Ca_2P_2O_7$ and calcium oxide. Therefore it is reasonable to believe that reactions occur between calcium phosphate compounds, such as $Ca_2P_2O_7$ and TCP, and the remaining calcium nitrates, carbonates and calcium oxide to form HAp. At 545°C, HAp is a major phase, along with trace amount of TCP.

For the ethanol-derived gel, a small amount of poorly crystallized hydroxyapatite is already present at 375°C (Fig. 5.2). No significant change in the XRD pattern occurs by increasing calcination temperature to 425°C or 445°C. At 460°C, poorly crystallized HAp and amorphous TCP are present. Crystallinity of HAp (as indicated by the peak width) significantly improves by increasing calcination temperature to 500°C (traces of

---

[8]The broad XRD peaks are considered as indicative of amorphous, partially amorphous, poorly crystalline or nanocrystalline character of the compounds; these descriptive words are used interchangeably; this is qualitative assessment and no attempt has been made to determine the degree of crystallization of the powders.

TCP are still present). Further increase in temperature to 545°C results in formation of phase-pure HAp (Fig. 5.2).

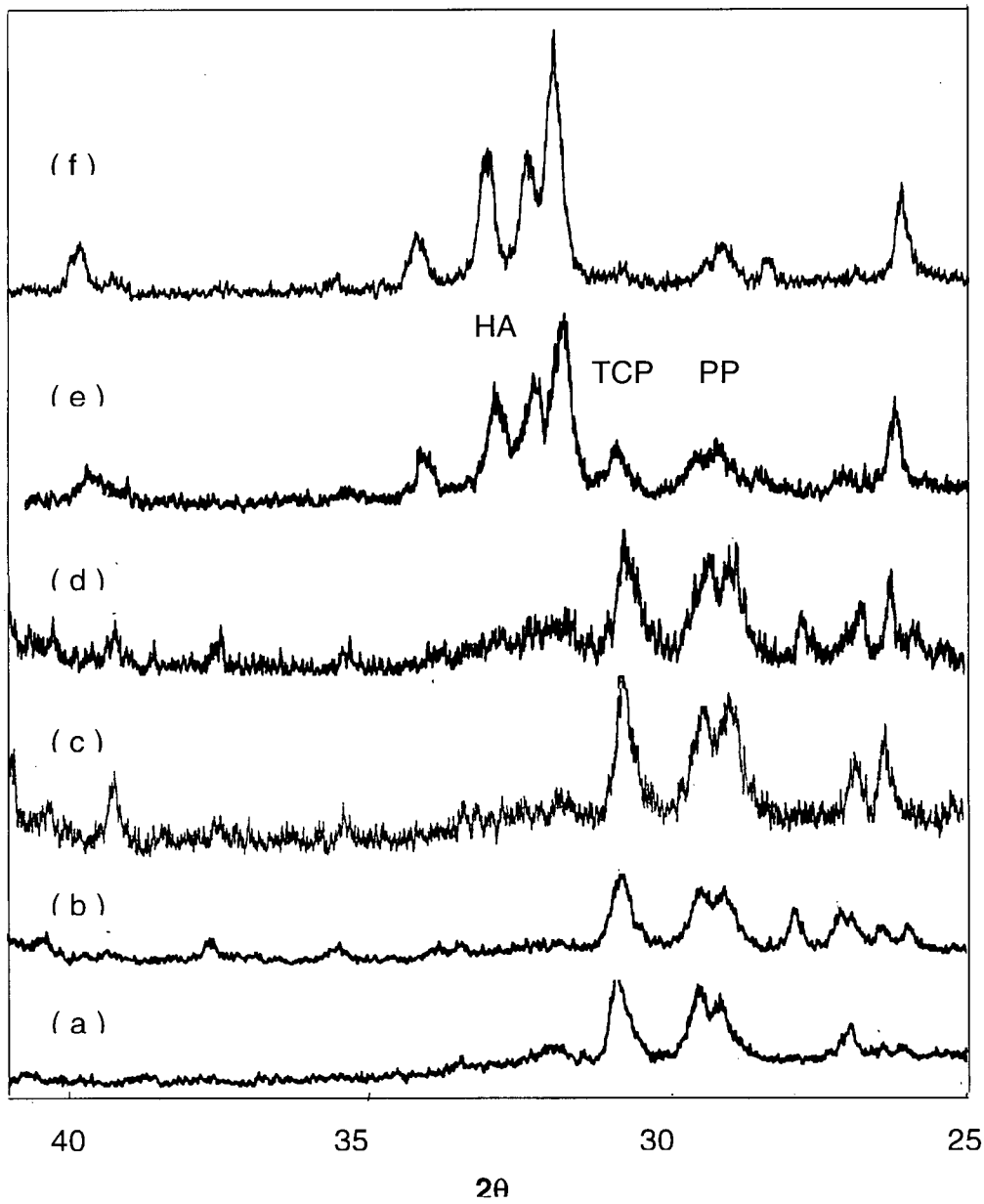


**Figure 5.1** XRD patterns for methanol-based gels calcined at (a) 375°C (b) 425°C, (c) 445°C, (d) 460°C, (e) 500°C and (f) 545°C.

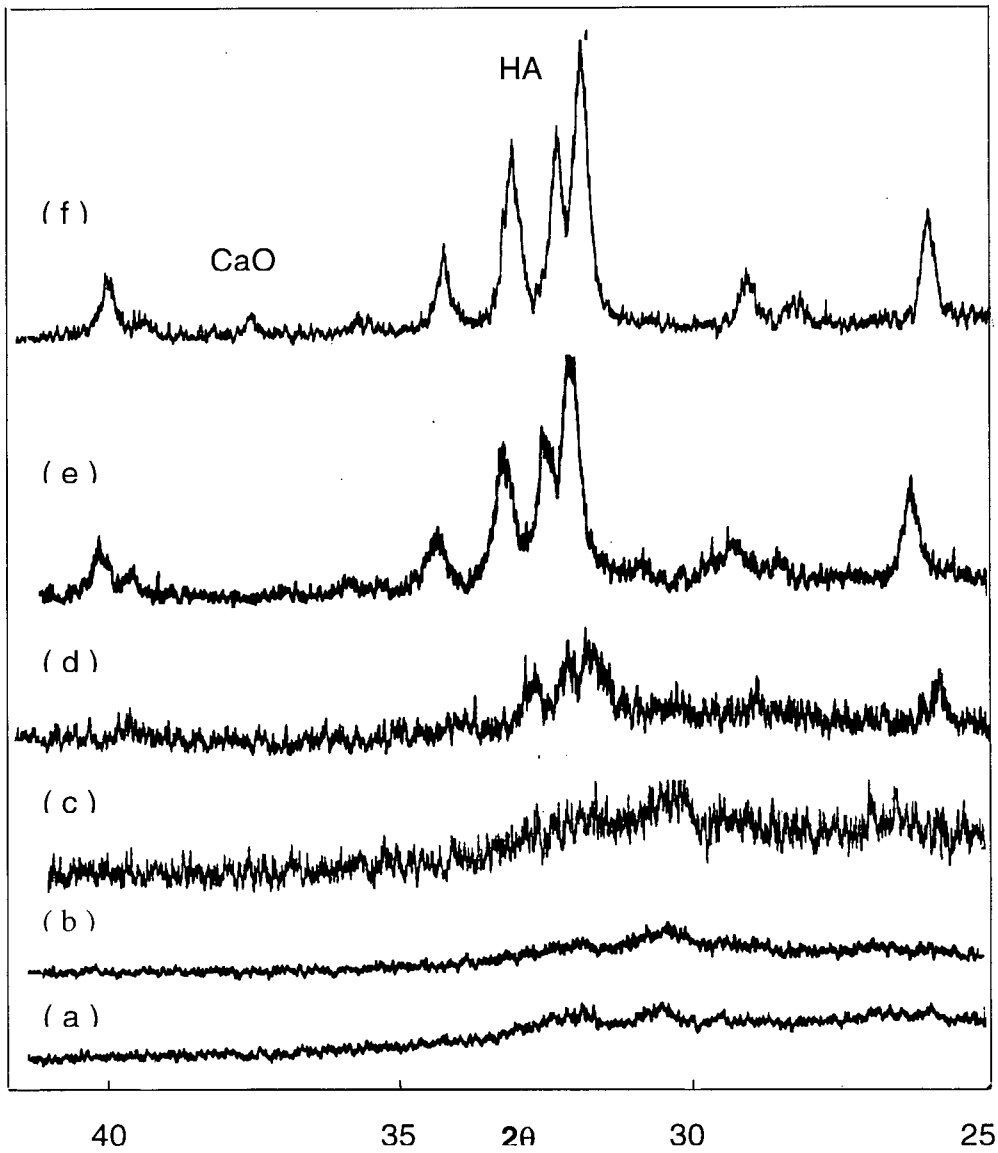


**Figure 5.2** XRD patterns for ethanol-based gels calcined at (a) 375°C (b) 425°C, (c) 445°C, (d) 460°C, (e) 500°C and (f) 545°C.

Well-crystallized calcium nitrate (CN) and amorphous apatite phases are present in propanol-based gel powder calcined at 375°C, Fig. 5.3. Upon increasing the temperature to 425°C the amorphous apatite crystallized into calcium phosphate compounds such as TCP and $Ca_2P_2O_7$. This trend continues till 445°C. At 460°C a poorly crystalline HAp develops while calcium nitrate TCP and $Ca_2P_2O_7$ are still

present. The crystallinity of HAp improves by increasing the temperature to 500°C, while trace amount of TCP is still present. The characteristic peaks of calcium nitrate are not present at this temperature. Calcination at 545°C results in a well-crystallized hydroxyapatite as evidenced by increased intensity and small half-intensity width of the characteristic reflection peaks. Trace amounts of TCP and calcium oxide are also present (calcium oxide has probably formed as a result of decomposition of calcium nitrate and other carbonated impurities).

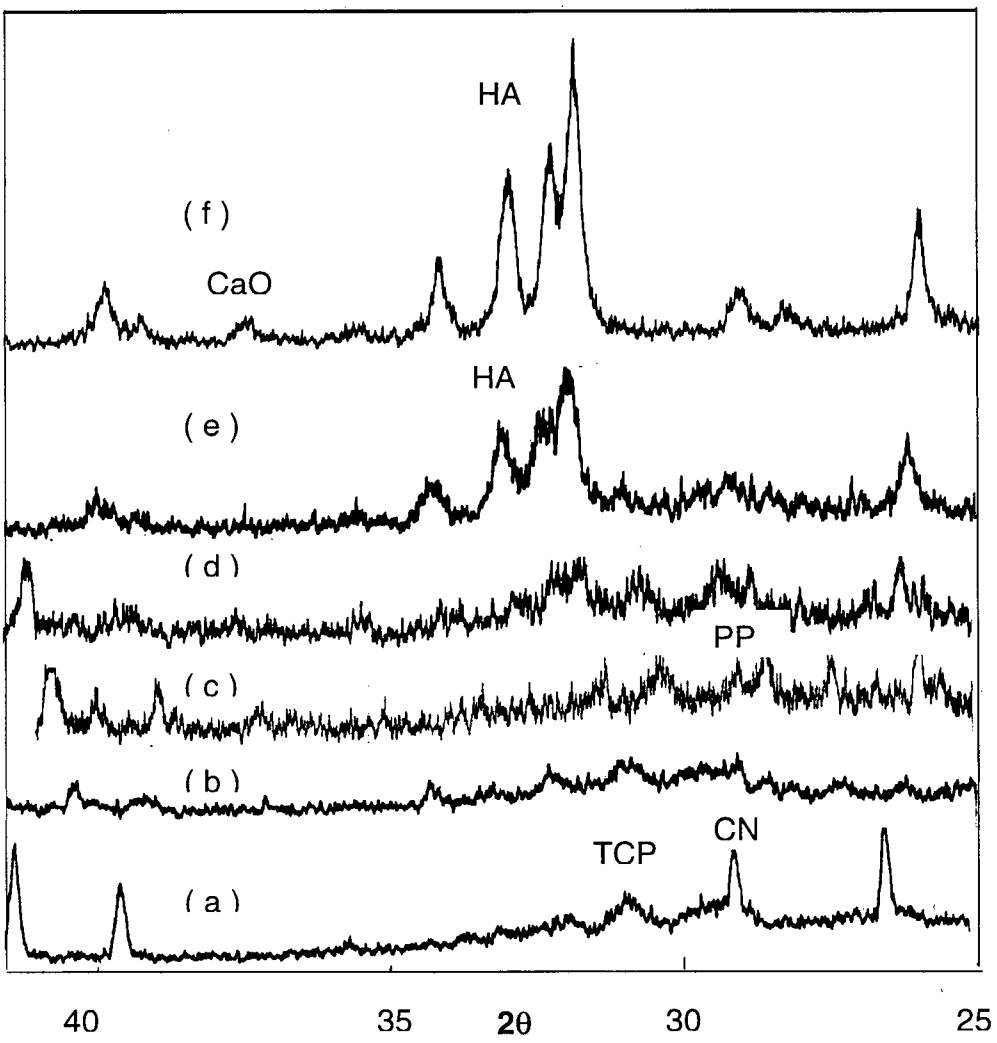


**Figure 5.3** XRD patterns for propanol-based gels calcined at (a) 375°C (b) 425°C, (c) 445°C, (d) 460°C, (e) 500°C and (f) 545°C.

### 5.1.1.b Thermal Analysis

The thermal gravimetric analysis (TGA) and differential thermal analyses (DTA) traces of the three samples are presented in Figs. 5.4 and 5.5, respectively. All the TGA curves start with a rapid weight loss between 100°C and 115°C, attributed to the evaporation and desorption of water and organic residues and are accompanied by endothermic effects in the DTA results. The slope of TGA curves changes at ~115°C (i.e. when weight loss stabilizes) which stays constant up to 420°C for both methanol and propanol-derived gels, and 460°C for the ethanol-based gel. This weight loss region bears small exothermic peaks, which are believed to be due to oligomerization and polycondensation of the hydrolysed species [51].

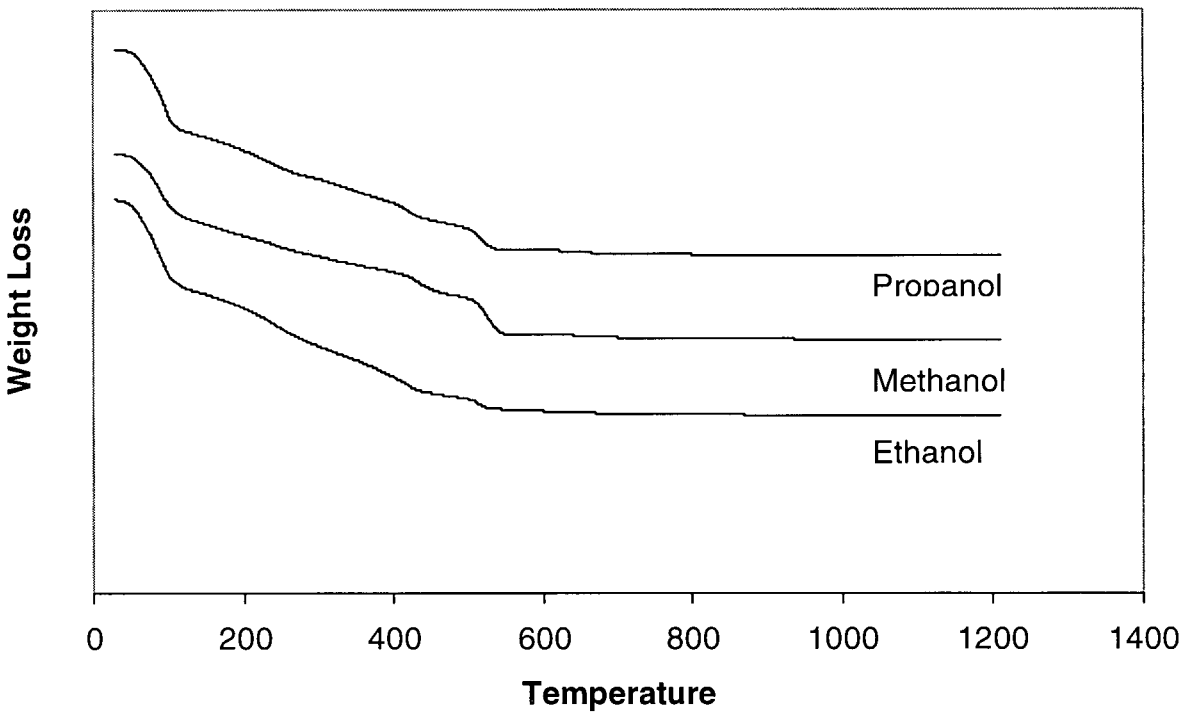


**Figure 5.4** Thermal gravimetric analysis of the dried gels.

A significant difference between the DTA curves for different solvent systems lies between 420 and 460°C, where an endothermic peak was detected for the methanol-

derived gel, whilst no specific peak was detectable for the ethanol-based gel. For the propanol-based gel, an exothermic peak was detected in this temperature region. The exothermic peak in the propanol-dried gel at 425°C is attributed to decomposition of the amorphous apatite to TCP and $Ca_2P_2O_7$. This effect can be also seen in the XRD patterns as the peaks related to TCP and $Ca_2P_2O_7$ appear in the XRD patterns after heating to 425°C. The TGA results also show a weight loss in this temperature range (420-460°C). The endothermic peak at 445°C in case of the methanol-derived gel can be attributed to crystallization of hydroxyapatite together with decomposition of calcium nitrate. This effect is also accompanied by a weight loss in TGA data.

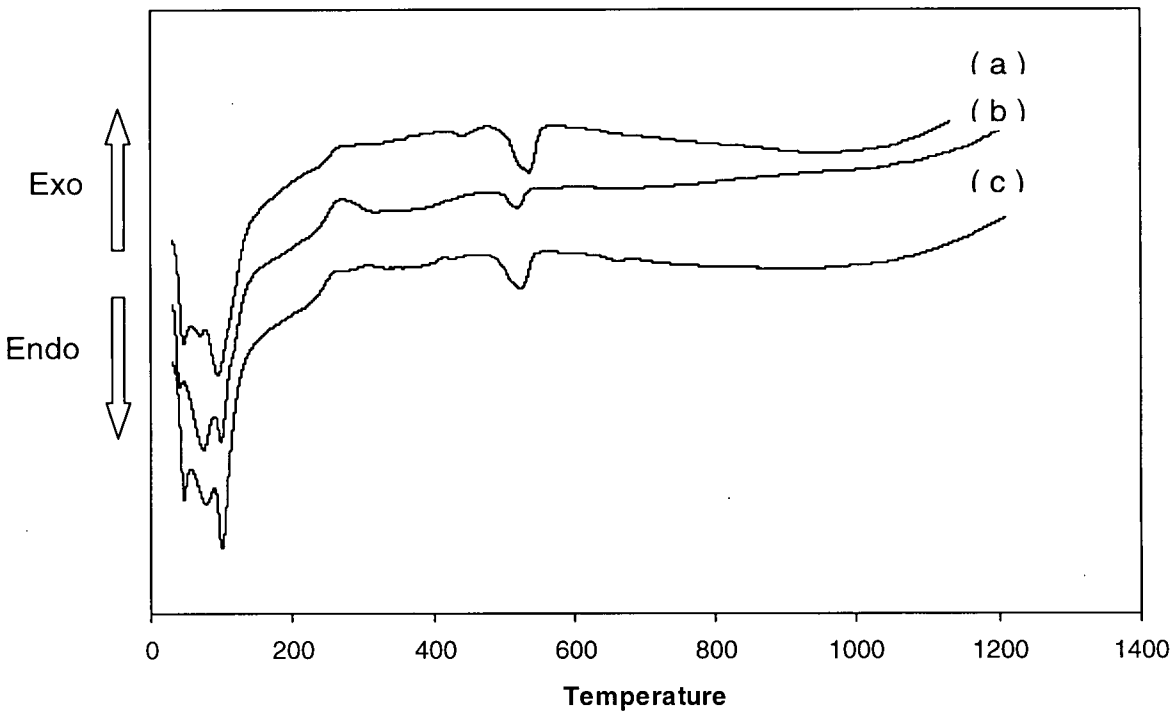


**Figure 5.5** Differential thermal analysis of the (a) methanol, (b) ethanol, and (c) Propanol-derived dried gels.

For all solvents, temperatures between 460°C and 510°C bear an exothermic drift in the DTA curves, which is represented by a slow weight loss. This exothermic drift can be assigned to crystallization of hydroxyapatite. This follows by an immediate endothermic peak with a minimum at around 530°C. This endothermic peak is

represented by rapid weight loss of the gels, which can be considered as a result of reaction between $Ca_3(PO_4)_2/Ca_2P_2O_7$ and calcium nitrate/carbonate to form hydroxyapatite. It is suggested therefore that hydroxyapatite forms from both the transformation of amorphous apatite phase and reactions among $Ca_2P_2O_7$, $Ca_3(PO_4)_2$, $CaCO_3$, and $Ca(NO_3)_2$, when the calcinations temperature reaches about 500°C. Although the exact pathway for the reaction of TCP and $Ca_2P_2O_7$ with other calcium compounds is not yet clear, the release of gaseous by-products of these reactions, i.e. oxides of carbon and nitrogen, is probably responsible for the weight loss observed.

### 5.1.1.c Electron microscopy

Figures 7a, 7b, and 7c are the scanning electron micrographs of methanol, ethanol and propanol-based gels calcined at 500°C, respectively.

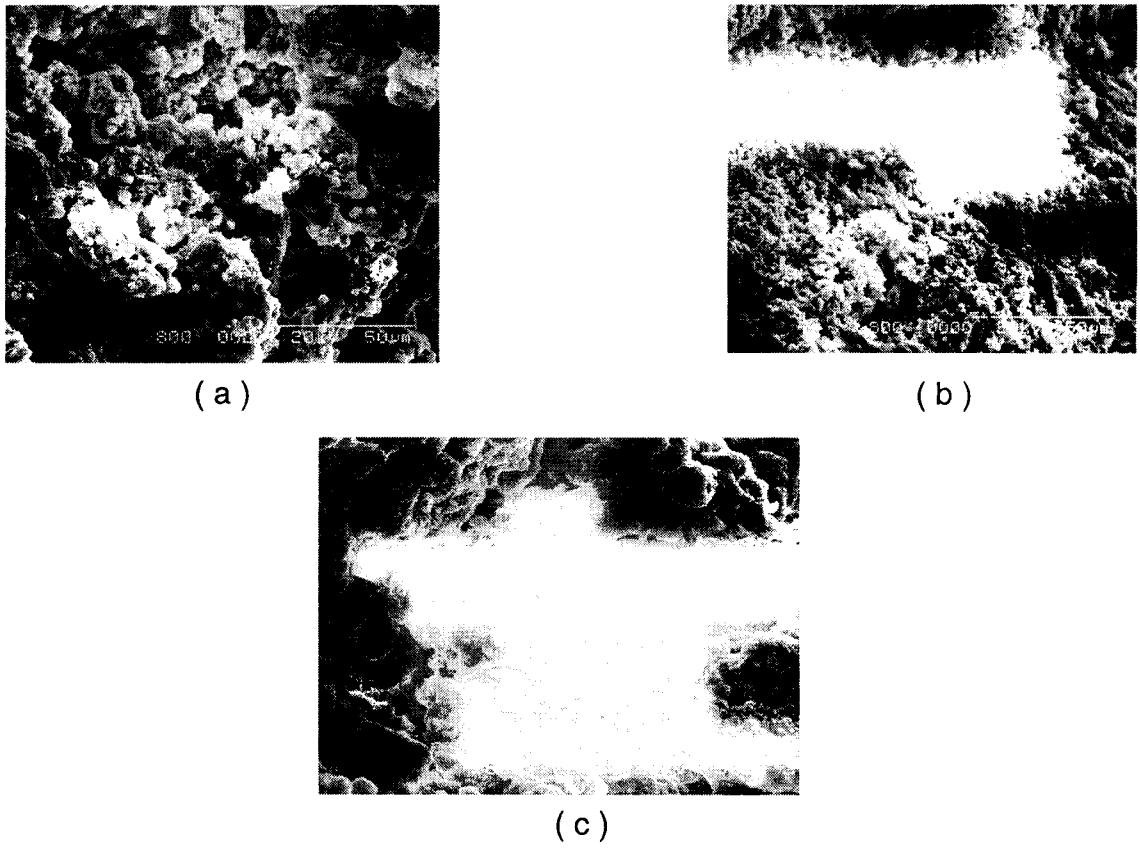

( a ) ( b )

( c )

**Figure 5.6** Scanning electron micrographs of (a) methanol-based, (b) ethanol-based, (c) propanol-based gels calcined at 500°C.

The micrograph of methanol-based gel after calcination at 500°C shows a porous structure with pore sizes in 5-20 μm range. A three-dimensional, amorphous-like, and highly porous structure is observed in the micrograph. Some crystal growth is observed on the background matrix. Fig 5.6b shows a porous morphology with the pore size ranging from 2 to 5 μm. The microstructure of the ethanol-based gel seems to consist of large agglomerates rather than a continuous amorphous-like structure, as observed in that of the methanol-based system. A porous, continuous structure is observed for the propanol-based gel calcined at 500°C (Fig. 5.6c) with the pore size ranging between 4 to 16 μm.

### 5.1.2 Discussion

It is obvious from the XRD data that the type of the alcohol (i.e. reflected through its molecular size) plays an important role on the phase evolution of hydroxyapatite in this sol-gel process. As the organic solvents and calcium nitrate have polar molecules, the solubility of calcium nitrate increases with the increase in the polarity of the alcohol solvent, which has been well recognized as a function of dielectric constant. The dielectric constants of propanol, ethanol and methanol are 20.1, 24.3 and 32.6, respectively, i.e., decrease with increasing molecular chain length. Therefore, the differences observed in the phase evolution of hydroxyapatite in different solvent systems can be attributed to the solubility of calcium nitrate in different organic solvents. The dissolution of calcium nitrate in the alcohol can be simply expressed as:

$$Ca(NO_3)_2 + xROH \rightarrow Ca(OR)_x(NO_3)_{2-x} + H^+ + xNO_3^- \qquad (5.1)$$

Better solubility of calcium nitrate in an alcohol, should result in larger x value in Eqn (1), due to higher dielectric constant of the organic solvent. It has been proposed previously that it would be more difficult for a calcium ion chemically bonded to a long-chain alcohol to interact with the hydrolysed alkoxide in the sol, due to, for instance, steric hindrance produced by the alkyl chains attached to calcium ion [64]. Liu et. al [50] have recently suggested that the hydrolysed phosphite can react with Ca precursor according to the following chemical pathway:

$$HPO(OC_2H_5)_{2-x}(OH)_x + Ca^{++} + NO_3^- \rightarrow \text{Ca-P intermediate} + H^+ \qquad (5.2)$$

where the Ca-P intermediate represents an amorphous phase, which is able to transform to apatite at elevated temperatures. They have suggested that if enough calcium ions react with hydrolysed phosphite then the Ca-P intermediate phase will form and will finally thermally transform into hydroxyapatite. In this case lower activation energy may be required for apatite formation.

Apatite can also be synthesized through the interactions among impure phases, such as $Ca_2P_2O_7$, $Ca_3(PO_4)_2$, $CaCO_3$ and $Ca(NO_3)_2$, as observed in the XRD results, where higher activation energy for the synthesis would be required. It is reasonable to believe that larger calcium-alcohol complex species $Ca(OR)_x(NO_3)_{2-x}$ retard the interaction with phosphorus alkoxide, necessary to form hydroxyapatite. The interactions among impure phases in order to form hydroxyapatite can be described by the following equation [50]:

$$\tfrac{1}{2}Ca_2P_2O_7 + Ca_3(PO_4)_2 + CaCO_3 + Ca(NO_3)_2 + 1/2H_2O \rightarrow Ca_5(PO_4)_3(OH) + CaO + 2NO_2 + CO_2 \qquad (5.3)$$

In the case of methanol-based gels calcined at 375°C, the presence of impure phases such as $Ca_2P_2O_7$, $Ca_3(PO_4)_2$, $CaCO_3$ and $Ca(NO_3)_2$ is expected due to incomplete reactions represented by equation (5.2). Therefore, better solubility of calcium nitrate in methanol, leading to large value of x in equation (5.1) could be the reason for more difficult interaction between Ca ions and hydrolysed phosphite, which will consequently leave equation (5.2) incomplete and will cause formation of impure phases at lower temperatures. However, these impure phases will further interact to form apatite at higher temperatures (Fig. 5.1).

It is hypothesized that intermediate solubility of calcium nitrate in ethanol compared to methanol leaves enough calcium ions to interact with hydrolysed phosphite and

therefore moves Eqn. 5.2 to the right. The presence of amorphous apatite phase in XRD patterns at low temperature supports this hypothesis. This amorphous, intermediate phase transforms into HAp upon increase in temperature as evidenced in Fig. 5.2.

The low solubility of calcium nitrate in propanol results in unreacted calcium nitrate, which in turn leads to incomplete reaction of calcium nitrate and hydrolysed phosphite, Eqn. 5.2. This will alter the mechanism of apatite formation toward the interaction among "impurity" phases (TCP, $Ca_2P_2O_7$) rather than crystallization from the amorphous phase. As it is evidenced from XRD results (Fig. 5.3), the well-crystallized calcium nitrate present at lower temperature will decompose into calcium oxide and $NO_2$ with further increase in temperature. A small amount of amorphous phase is also present at low temperatures (375°C), which decomposes into TCP and $Ca_2P_2O_7$ at 425°C. These "impurity" phases will further react at higher temperatures to form hydroxyapatite. Decomposition of calcium nitrate provides calcium for calcium phosphate compounds such as TCP and $Ca_2P_2O_7$ to form hydroxyapatite (Fig. 5.3).

The endothermic peak observed in the range of 500-550°C in DTA curves of all the samples (regardless of the solvent) is representative of final HAp formation either through crystallization process or chemical interactions among different phases. As shown in Fig. 5.5, there is less energy required to form HAp in an ethanol-base system as compared to methanol- or propanol-based systems, as smaller endothermic peak appears at this temperature range. This effect is produced due to different formation pathways which is consistent with the results of Liu et. al. [82]. In their work they have speculated that crystallization of the amorphous intermediate phase in order to form HAp requires less activation energy compared to interaction of impure phases.

The crystal size of the gels calcined at 500°C was calculated using the Scherrer equation:

$$\Delta(2\theta)=0.9\lambda/D\cos(\theta) \qquad (5.4)$$

Where $\Delta(2\theta)$ represents the peak width at half maximum intensity of the reflection (002), $\lambda$ is the wavelength for $CuK_\alpha$ ($\lambda$=0.15418 nm), and $D$ is the crystal size (nm).

This approximate calculation reveals that the crystal size of HAp formed in different solvents and after calcinations at 500°C follows the order of methanol (~50nm) > propanol (~40nm) > ethanol (~30nm).

Although, due to the large number of parameters that influence different stages of this complex sol-gel process, suggesting a conclusive reason for the observed phenomena, using the characterization methods applied here, is impossible but it seems that phase evolution and crystal size in different solvent systems is probably affected by the ability of the alkyl group from alcohol solvent to substitute the OEt groups of the phosphorous precursor. The interchange between two alkyl groups can be expressed as follows:

$$HPO(OH)_x(OEt)_{2-x} + yROH \rightarrow HPO(OH)_x(OEt)_{2-x-y}(OR)_y + y\ EtOH \quad (5.5)$$

where ROH can be methanol, ethanol or propanol. According to Livage et. al. [83], both the entropy and enthalpy of the new molecular species will change upon such substitution, leading to a change in chemical reactivity towards hydrolysis and condensation reactions, thus affecting the morphology and the of the final gel [83]. It is therefore expected that in the process studied in this thesis $OCH_3$- substitution for $OC_2H_5$- group and also substitution of $OC_3H_7$- for $OC_2H_5$- changes the rate of hydrolysis and condensation reactions and therefore results in different HAp formation pathways as well as different gel morphology and crystal size. SEM observations confirm this hypothesis.

Scanning electron microscopy (Fig. 5.6a, 5.6b and 5.6c) shows a porous, continuous three-dimensional structure for both methanol and propanol-derived gels. However, the ethanol-derived gel shows somewhat different particulate morphology consisting of smaller pores and agglomerate particulates rather than a continuous, three-dimensional structure. Such difference can be attributed to different chemical pathways during phase evolution. In the case of methanol and propanol systems, formation of crystalline intermediate phases such as TCP and $Ca_2P_2O_7$ and calcium carbonates, their interaction and release of gaseous by-products (especially $CO_2$) results in larger pore size, as evidenced in Figs. 5.6a and 5.6c Moreover, similar phase evolution

pathway in methanol and propanol-based systems observed in this study might be the cause for similar morphologies of calcined gels observed in these two systems. For the ethanol-derived gel the main mechanism of HAp formation appears to be via crystallization from an amorphous intermediate phase, which results in less porosity in final calcined gel as well as a particulate structure as obvious in Fig. 5.6b.

## 5.2 HAp coating characterization

### 5.2.1 Coatings on titanium substrates

#### 5.2.1.a Electron microscopy examination

The substrate surface preparation techniques included chemical treatment and sand blasting. Figure 5.7a is the electron micrograph of the surface of titanium plate, chemically treated with phosphoric acid. The surface dissolution reaction has resulted in formation of a roughness in a range of 2-3 μm on the surface. Figure 5.7b presents the titanium surface after the alternative surface preparation method of sandblasting. The surface thus produced has a high roughness of about 10 μm.

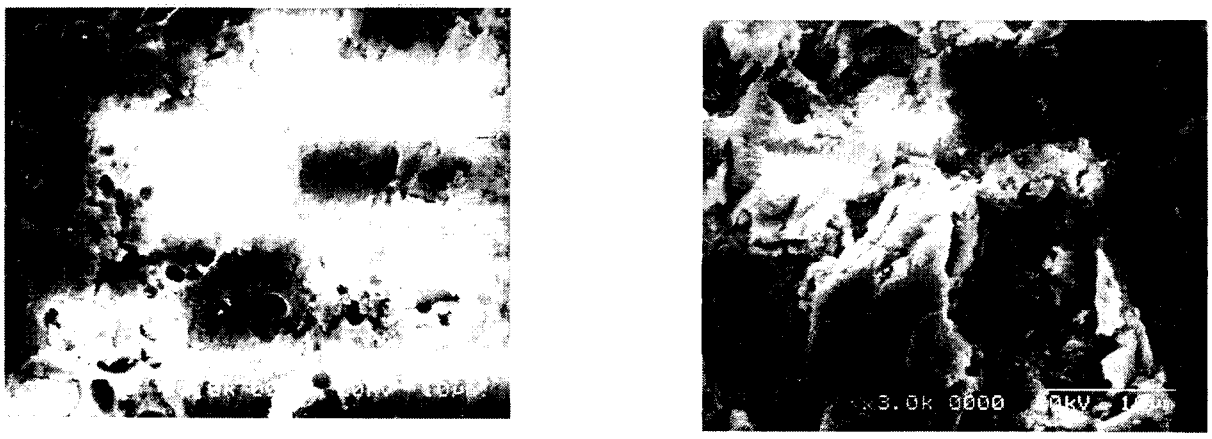


( a ) ( b )

**Figure 5.7** Scanning electron micrograph of (a) surface of titanium plate, treated with phosphoric acid, and (b) titanium surface after sandblasting.

Figure 5.8a, 5.8b, and 5.8c show the chemically treated titanium substrates after spin coating with methanol, ethanol, and propanol-based sols, respectively. The coating surface finish follows the morphology of the substrate's surface regardless of the

solvent employed. The coating is transparent to the electron beam and therefore the substrate surface features can be easily seen under the coating layer. The coatings based on all three solvent systems provide a good coverage of the surface, while some microcracks (1-2 μm) are observed in the films. These cracks are much less extensive as compared to those produced by plasma spraying [80,84] and are probably formed due to drying and sintering strain of thicker sections of the coating filling the rough surface features.

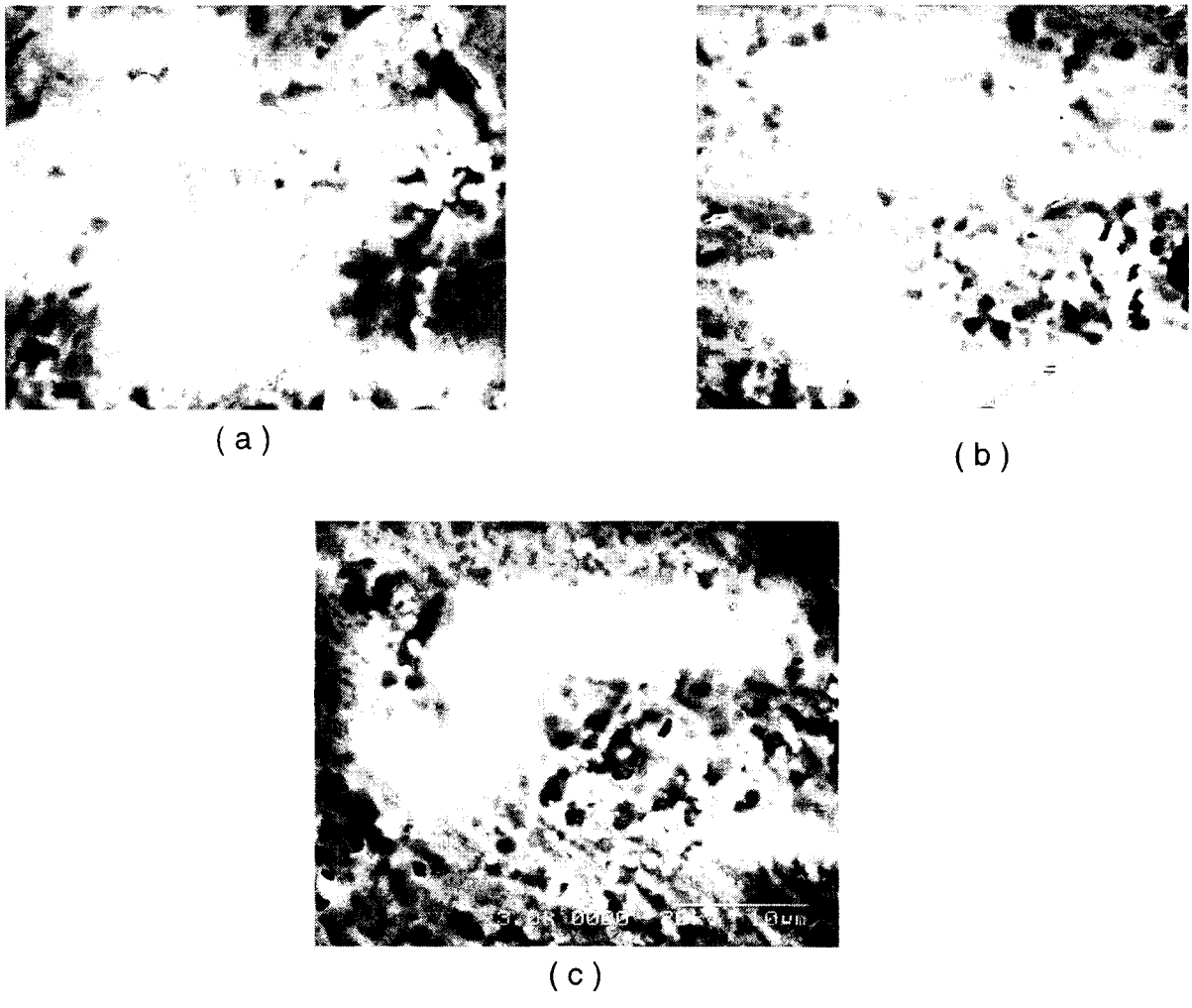

**Figure5.8** Surface of chemically treated in phosphoric acid (85%) at 50-60°C for 30 minutes titanium substrates after spin coating with (a) methanol, (b) ethanol, and (c) propanol-based solutions.

Figures 5.9a-d show the EDS results of the titanium etched surface and titanium surface after coating with methanol, ethanol and propanol-based sols, respectively. The appearance of calcium and phosphorous peaks in the EDS spectra after the coating deposition is an indication of the presence of an apatite layer on the surface.

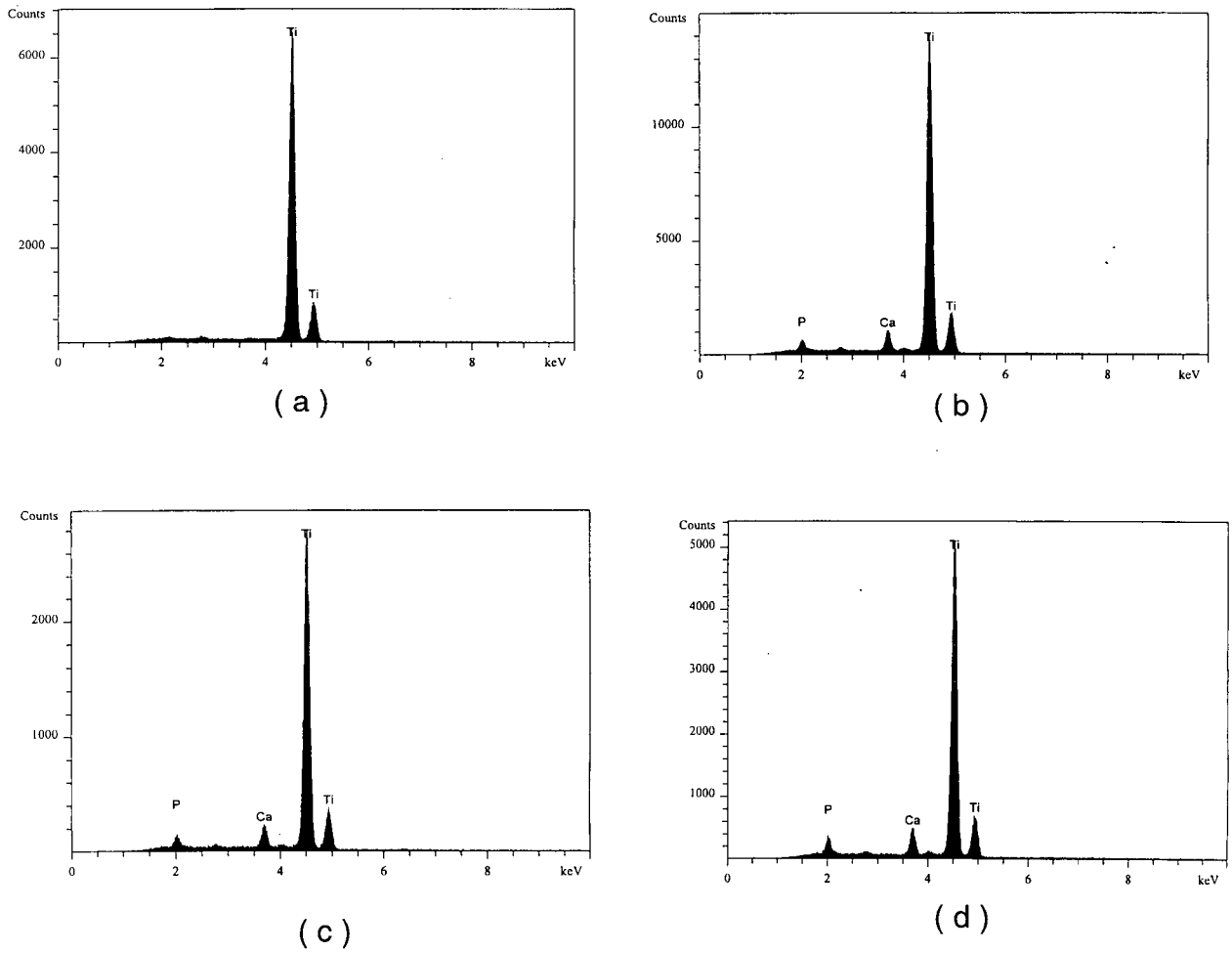


**Figure 5.9** Energy dispersive spectrometry of (a) titanium etched surface and titanium surface after coating with (b) methanol, (c) ethanol and (d) propanol-based solutions.

Figure 5.10a-c show the sandblasted titanium surfaces after coating with solutions obtained from methanol, ethanol and propanol solvent systems, respectively. It is

obvious from the picture that the extent of microcracking increased with the size of the alcohol molecule used as the diluting media for solution preparation. These cracks are mainly observed in the thicker pockets in cavities formed by surface irregularities. The solution's flow from the top of these irregularities toward the substrate surface produced a reservoir for coating solution inside these cavities and thus a ticker layer of coating formed in these areas. Features resulting from this down-flow of the solution are clearly observed in the propanol-based coated surface (Fig 5.10c). Thicker coating translates to more drying and sintering strain in direction parallel to the substrate surface, which will finally results in microcracking. With increase in the molecule size of the alcohol solvent, the viscosity and molecular weight of the solution increases. This effect will further increase the solution flow toward the above mentioned cavities and therefore a thicker layer of coating will form, which is more susceptible to cracking after heat treatment, due to larger strain.

( a )

( b )

( c )

**Figure 5.10** Sandblasted titanium surfaces after coating with solutions obtained from (a) methanol, (b) ethanol and (c) propanol solvent systems.

Both chemical surface preparation and sandblasting, applied to improve coating adhesion to the substrate by increasing mechanical interlocking, yielded good coating coverage on the substrates' surfaces. Chemical treatment produces surface features with less roughness compared to sandblasting, and results in a more uniform coating thickness and finally leads to less microcracking. Practically, chemical treatment is the only method viable for smaller objects, such as stents.

### 5.2.1.b Infrared spectroscopy

Figure 5.11 shows the FTIR spectra of the surface of sandblasted Ti substrates coated with methanol, ethanol and propanol-based solutions and fired at 500°C for 10 minutes. The characteristic $\nu_4$ $PO_4$ bands at 560 $cm^{-1}$ and 600 $cm^{-1}$, $\nu_1$ band at 1000 $cm^{-1}$ and a $\nu_3$ $PO_4$ absorption band at 1070 $cm^{-1}$ are observed, which are typical of apatitic structure [64]. Short-range atomic arrangement in the apatite structure is responsible for the diffuse shape of the peaks [64], although all the peaks are clearly distinguishable. This effect is produced due to the short dwelling time of the samples at the heat treatment temperature, i.e. poor crystallinity of the structure. Increasing the soaking time at 500°C would result in an improved molecular arrangement and higher crystallinity HAp. A small peak at 620 $cm^{-1}$ can be assigned to OH group, indicating the presence of bonded water in the film structure [45]. The broad bands at 1429 $cm^{-1}$ and 1494 $cm^{-1}$ are attributed to carbonate groups. The broad nature indicates the possible presence of organic species such as $-CH=CH_2$ or -COO- groups formed due to reactions between the evolved organics and calcium [28]. The small peak observed at 860 $cm^{-1}$ on the methanol and ethanol spectra is also related to $CO_3$ groups, suggesting carbonates substitution for $PO_4$ group in the apatite structure. Therefore, the coatings can be considered as carbonated apatite, similar to the structure of natural bone.

Comparing $PO_4$ bands in the range of 500-600 $cm^{-1}$, the sharpness of characteristic peaks decreases with the size of alcohol molecule, i.e. methanol>ethanol>propanol. Considering the short dwelling time of the samples at the firing temperature (10 minutes) the rate of organic residue desorption and decomposition plays an important role in the rate of apatite formation. Therefore, faster desorption of smaller organic

molecules (i.e. in methanol solvent) might be a reason for faster arrangement of apatitic structure. Surface features (e.g. roughness) are responsible for the background noise observed in the FTIR spectra.

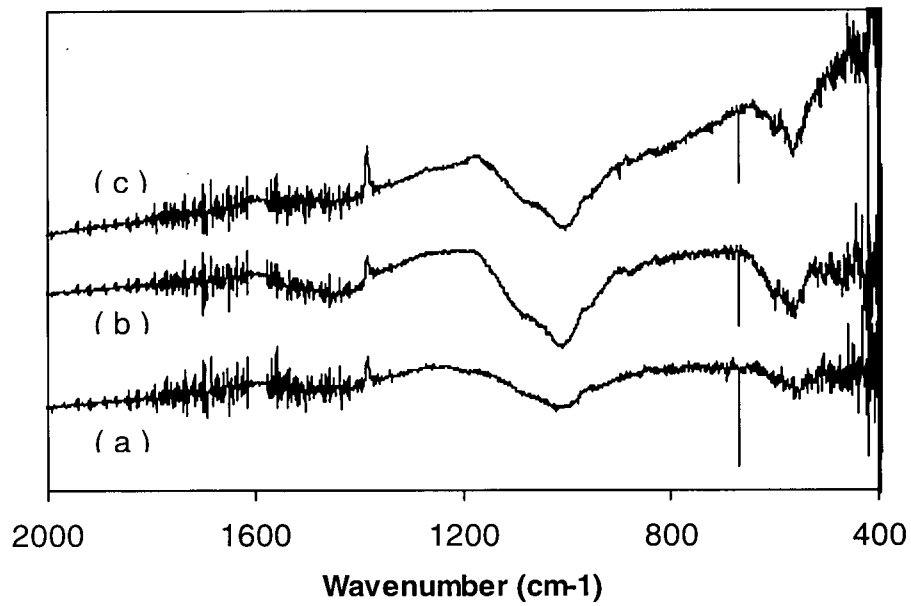


**Figure 5.11** FTIR spectra of the surface of sandblasted titanium substrates after coating with (a) methanol, (b) ethanol and (c) propanol-based solutions.

### 5.2.1.c In-vitro bioactivity test

The HAp coated titanium substrates were submerged in a simulated body fluid (SBF), which has the same ionic components as those found in human blood plasma (detailed in Appendix I), for 7 days at ambient temperature. Precipitation of HAp from the SBF in such a test is considered as indicative of bioactivity of the exposed surface [80]. Figures 5.12a, 5.12b and 5.12c show the SEM micrographs of surface morphology of titanium substrates coated with methanol, ethanol, and propanol-based sols, respectively, after incubation in SBF. Scattered ball-like apatite grains appeared on the surface after the incubation. Microcracks and disintegration of the coatings are also observed in the vicinity of the newly formed grains. The occurrence of these cracks and ball-like apatite deposits is believed to be a result of dissolution-reprecipitation process between the HAp coating surface and the SBF solution. The similar effect and

microstructure of the ball-like apatite grains have been observed for plasma sprayed calcium phosphate coatings studied by Liu et. al. [80], under similar SBF incubation conditions, and considered as an evidence of formation of apatite structure.

The newly formed apatite layer is scattered on the surface in the form of clusters of ball-like grains. The grains are equiaxial, with an average diameter of 2.5 μm, in all the samples (Figs. 5.12a-c). The HAp "balls" seem to have a porous structure, consisting of agglomerates of smaller particles. No apparent difference in apatite formation was observed for titanium substrates coated with solutions made with different organic solvents. This in-vitro test and formation of the apatite layer on the surface of the HAp coated substrate confirms the bioactive nature of the coatings.

( a )

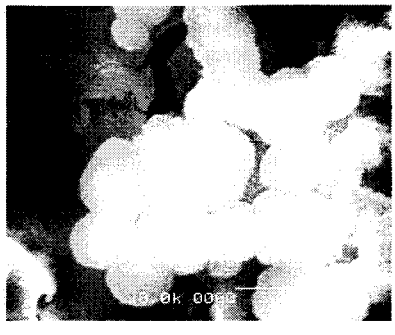

( b )

( c )

**Figure 5.12** SEM micrographs of surface morphology of titanium substrates coated with (a) methanol, (b) ethanol, and (c) propanol-based solutions, after incubation in SBF.

### 5.2.2 Stainless steel substrates

#### 5.2.2.1 Stainless steel wires

As no previous attempts of coating stainless steel wires have been reported, the coating process has been optimized on trial-and-error basis. In this section the results obtained through this process are presented in the sequence of (a) surface treatment, (b) solution effect and coating process, and (c) firing conditions.

#### 5.2.2.1.a surface treatment

The wires were acid-etched to produce surface roughness to enhance adhesion of HAp coatings to the wires. Figures 5.13a-d show the stainless steel wires after exposure to different acidic reagents in order to produce surface roughening. All the etched samples were treated in acidic solution of 50 vol% of hydrochloric, phosphoric and nitric acids in water, for 40 minutes at a temperature between 60-70°C. Figure 5.13a shows the surface of the as-received stainless steel wire. Surface features resulted from rolling and greasy spots remained from finishing processes can be observed on the surface. The greasy spots are removed from the surface although no sign of etching is observed after exposure to nitric acid solution as shown in Fig. 5.13b. Phosphoric acid produces slight surface roughening in the form of surface grooves (Fig 5.13c) while hydrochloric acid (HCl) results in extended surface roughening in form of grooves and grain boundary corrosion (Fig. 5.13d) after similar etching procedure. Nitric and phosphoric acids do not seem suitable for surface treatment of stainless steel wires due to their slight etching effect considering the long time and relatively high temperature of exposure. The corrosion effects produced by HCl offers the possibility of controlling the etching parameters such as time and temperature in order to produce an optimized surface roughness suitable for the subsequent coating procedure.

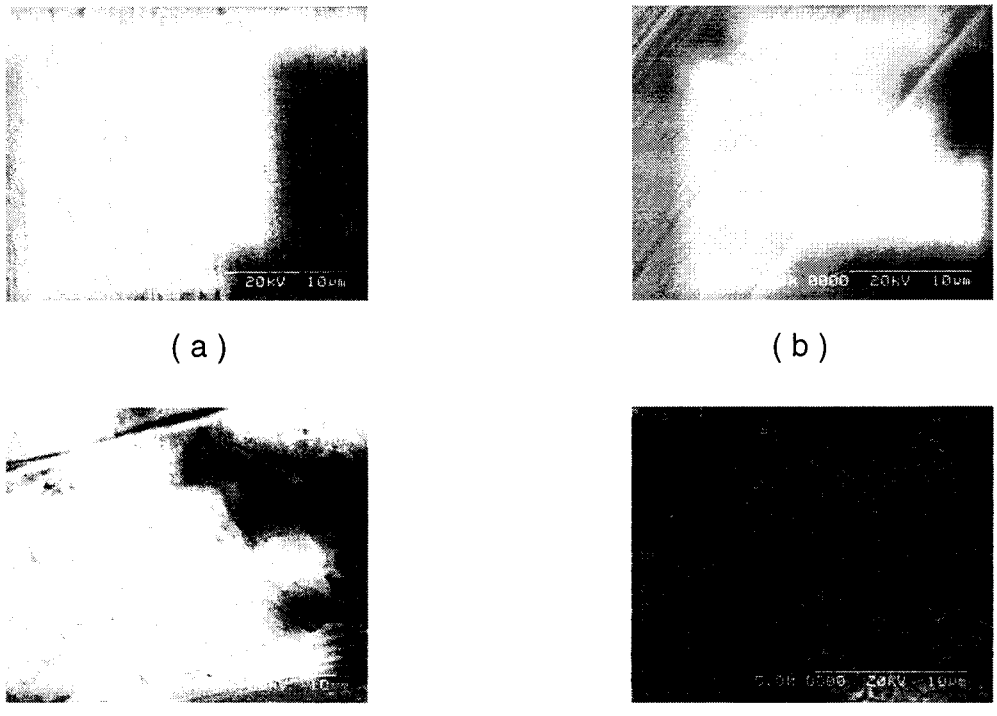

( a ) ( b )

( c ) ( d )

**Figure 5.13** SEM micrographs of (a) as received stainless steel wire and wires after exposure to (b) nitric acid, (c) phosphoric acid, and (d) hydrochloric acid.

In order to investigate the effect of time of HCl exposure on the surface roughness, stainless steel wires were etched for periods of 10, 20, 30, 40, 50 and 60 minutes. The SEM micrographs of these samples are presented in Figures 5.14a-f, respectively. The effect of HCl on the surface starts with attacking the grain boundaries, which continues up to 30 minutes of exposure, when grain corrosion starts producing a rougher surface (Figs. 5.14a-c). Further corrosion of the surface occurs on the grain surfaces rather than the grain boundaries, as shown in Figs. 5.14d-f.

( a ) ( b )

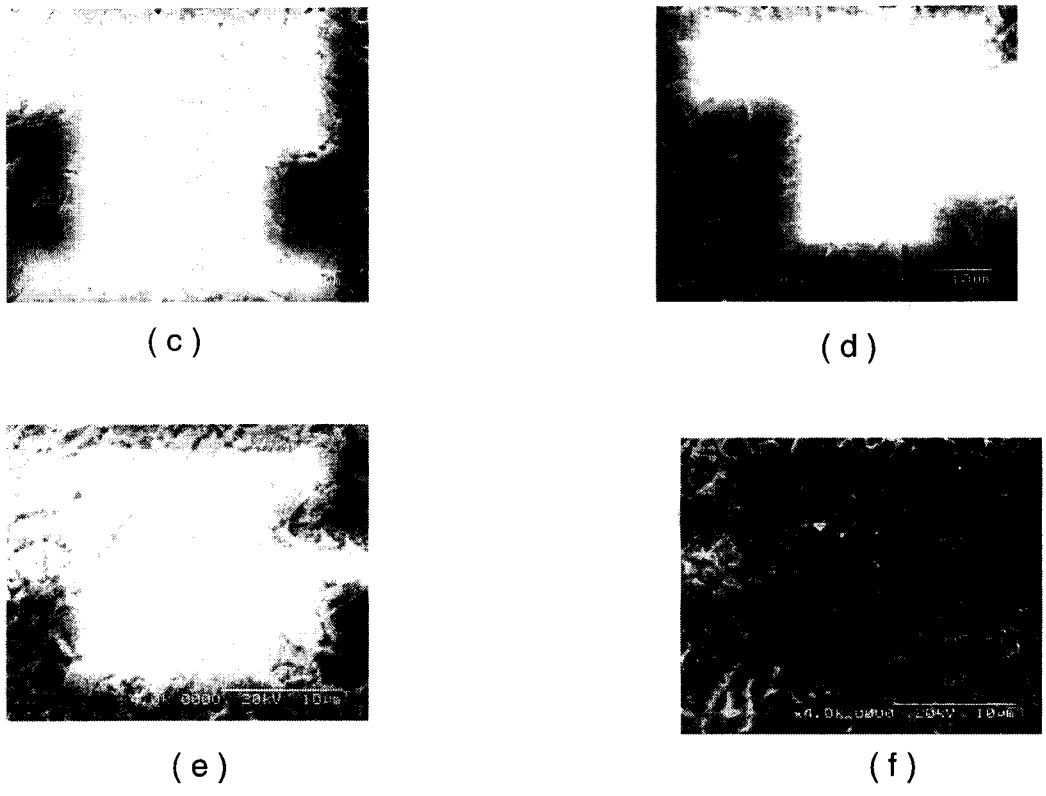


**Figure 5.14** SEM micrographs of stainless steel wires treated with HCl (2.4 N) for (a) 10, (b) 20, (c) 30, (d) 40, (e) 50, and (f) 60 minutes at 75°C and neutralized for 4 minutes.

As only slight degree of surface corrosion is believed to be necessary for coating purposes, and in order to reduce the damage produced by chemical treatment, 10 minutes etching in HCl at 70°C was chosen as the pre-treatment process. Immediately afterwards the samples were neutralized in a process described earlier.

#### 5.2.2.1.b Effect of coating solution

The effect of the coating solution has been examined in the two following sections. First the effect of organic solvents on the coating properties of the hydroxyapatite sol was investigated. Study of the effects of solution concentration follows as the second section.

**Effect of the organic solvents**: It has been pointed out by Brinker and Sherer [12] that the deposited film thickness ($h$), obtained through dip coating in low viscosity solutions is dependent on the substrate withdrawal speed ($U$), liquid viscosity ($\eta$), liquid-vapour surface tension ($\gamma_{LV}$), and gravity forces ($\rho gh$):

$$h = 0.94(\eta U)^{2/3}/\gamma_{LV}^{1/6}(\rho g)^{1/2} \qquad (5.6)$$

In coating stainless steel wires with sols prepared with different solvents, parameters such as $U$ and $\rho g$ are kept constant in all the experiments. The remaining parameters, such as $\gamma_{LV}$ and $\eta$, are affected by the solvent and therefore are variables. Due to the high complexity of the system, caused by presence of various components in the solution (water, organic solvent, calcium nitrate and triethyl phosphite), quantitative analysis of the effect of the solvent on the film thickness and coating properties is very difficult. Therefore, the effect of theses variable parameters are investigated qualitatively using SEM images.

Figures 5.15a-c show the picture of bent stainless steel wire samples, dip coated with hydroxyapatite sols prepared from methanol, ethanol and propanol-based solutions, respectively. The wire samples are unbent before microscopic investigation, to observe the coating behaviour in simulated stent deformation experiment. Cracking and delamination is observed at the bending point of the methanol-based coated sample (Fig. 5.15a) while only slight microcracking is observed in the vicinity of the bending point. The coating remains intact in all the other areas on the surface of the wire. Accumulation of the coating solution in the bent section has resulted in an excessively thick coating in this area. This thicker layer is more prone to cracking due to residual drying and sintering strain and the resulting microcracks pre-existing in this layer, which will finally lead to cracking and delamination during unbending. For the ethanol-based coating, delamination, cracking and disintegration is observed in the bent section, probably due to a thicker accumulated layer, Fig. 5.15b. Larger extent of cracking and disintegration is observed in the propanol-based coating (Fig 5.15c). The cracks are present in the vicinity of the bending point as a result of stress in the coating layer.

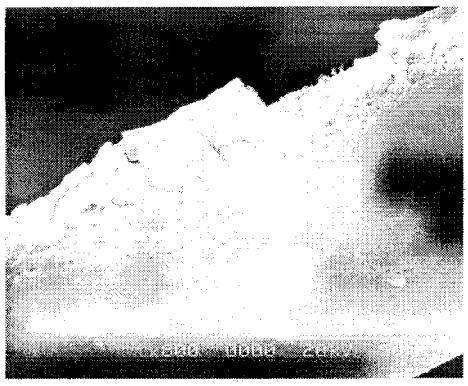

( a )

( b )

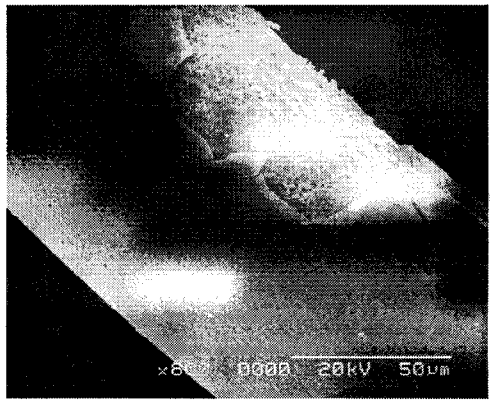

( c )

**Figure 5.15** SEM micrographs of bent stainless steel wire samples, dip coated in (a) methanol, (b) ethanol, and (c) propanol-based solutions after unbending.

As observed in figures 5.15a-c the extent of cracking and coating disintegration after unbending increases with the size of alcohol molecule. This can be explained by the effect of the solvent on the solution viscosity and surface tension, which will finally affect the film thickness, especially in a V-shape substrate such as a bent wire. A thicker layer is more prone to cracking due to residual stresses of drying and sintering. A solvent with a larger molecule size increases the thickness of the coating at the bending point, resulting in more cracking after unbending. Consequently only methanol and ethanol-based solutions are chosen for further examinations.

**Effect of solution concentration:** Figures 5.16a and 5.16b show the pictures of bent wire samples coated with dilute (1M) methanol and ethanol-based solutions, respectively. Compared to figures 5.15a and 5.15b, the effect of solution accumulation at the bending point and the extent of microcracking are significantly reduced. By increasing the amount of solvent used to prepare the sol (i.e. diluting the sol), the viscosity of the solution decreases, which will also decrease the thickness of the coating according to equation 5.6. Reduced thickness of the coating layer results in less strain caused by shrinkage during drying and sintering, in direction parallel to the substrate (for sub micron sol-gel films most of the drying plus sintering strains appears to be in direction normal to the substrate, and this component of strain does not produce stress in the film). Therefore less cracking is observed in the final film.

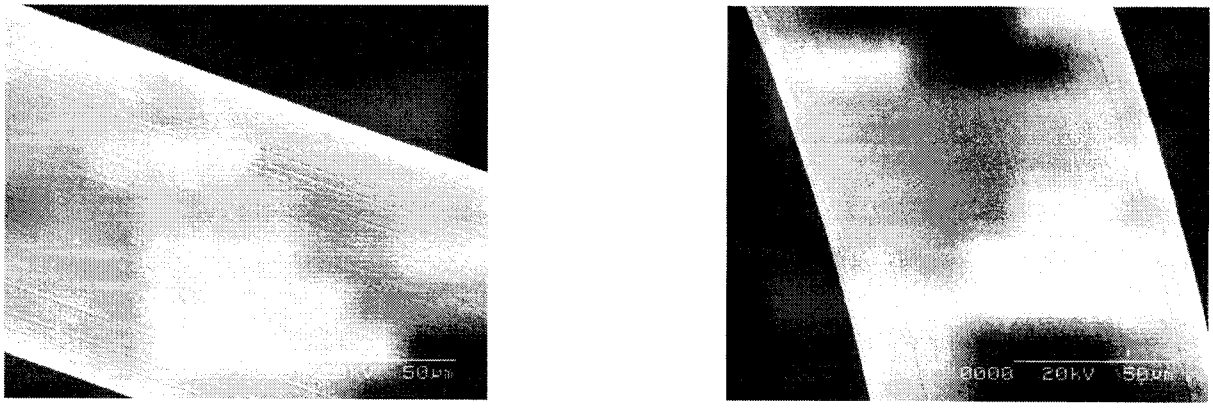

( a ) ( b )

**Figure 5.16** SEM picture of bent wire samples coated with dilute (1M) (a) methanol, and (b) ethanol-based solutions after unbending.

### 5.2.2.1.c Effect of heat treatment time

Figures 5.17.a-c show the bent portion of stainless steel wires coated with dilute (1M) methanol sol after firing for 10, 30 and 60 minutes at 500°C, respectively. The samples were unbent before SEM investigations, in order to simulate system deformation during stent placement. After 10 minutes firing, some crystallization of the thicker layer at the

bending point is observed (as described earlier the thicker layer is a result of excess amount of solution trapped in the bent area during dip coating). However, no excessive cracking or disintegration is observed, Fig. 5.17a. By increasing the firing time to 20 minutes, enhanced cracking results in the disintegration and removal of the coating. This damaged area has a size of ~50 μm. No further cracking is observed in the adjacent thinner coating, Fig 5.17b. Significant cracking is observed on the bent area of the sample fired for 60 minutes. The damaged (cracked and delaminated) area is about 100μm in length. The degree of damaged produced after unbending coated wire samples increases with the increase in firing time.

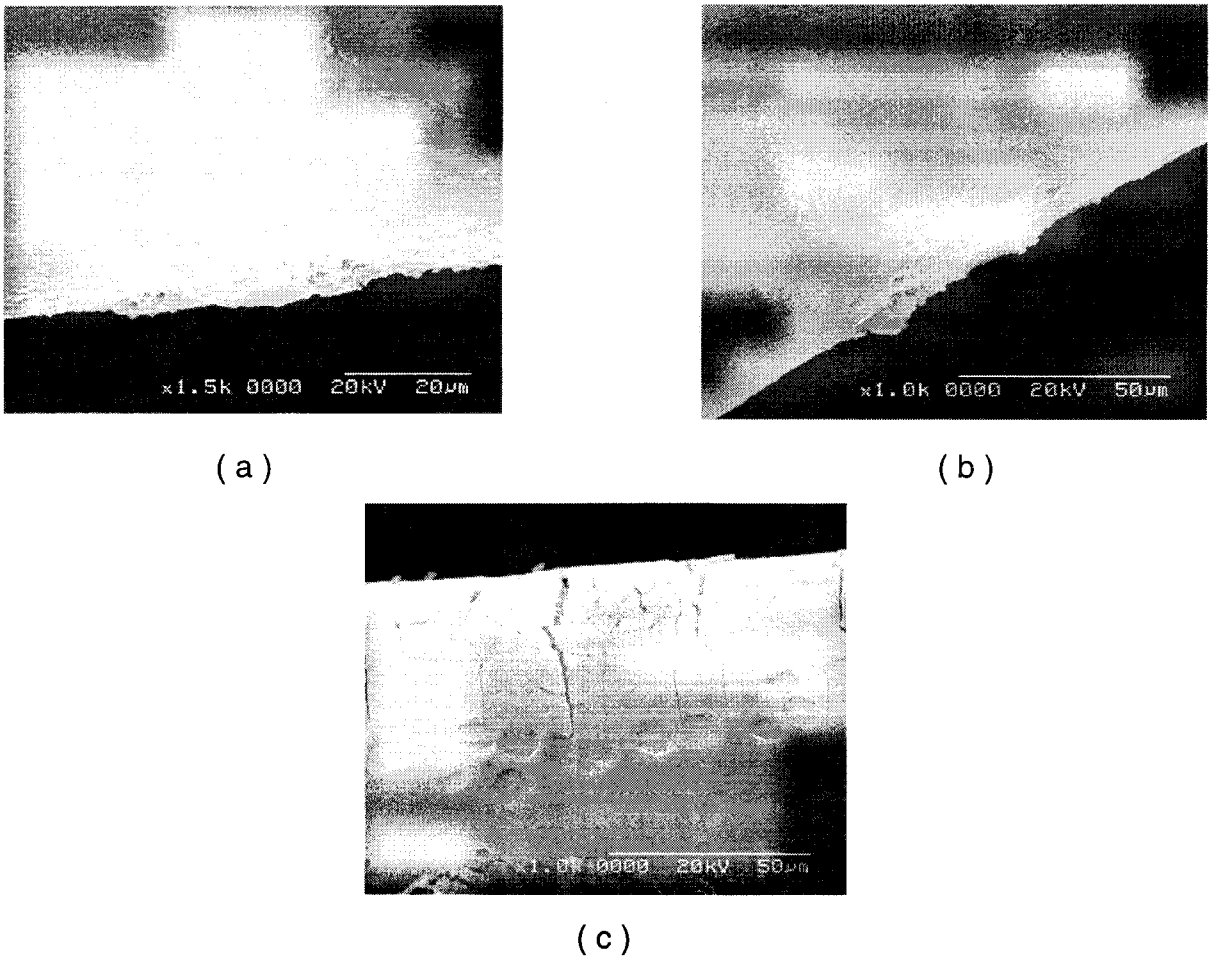


**Figure 5.17** SEM picture of unbent stainless steel wires coated with dilute methanol solution and fired for (a) 10, (b) 30, and (c) 60 minutes at 500°C.

To examine the extent of crystallization of the coatings after various heat treatment times, XRD was conducted on similarly heat-treated thin films of the sols on glass substrates. Figure 5.18 shows the phase evolution of hydroxyapatite after different firing time periods at 500°C. 10 minutes of heat treatment produces a highly amorphous apatite thin film. Increasing the firing time to 30 and 60 minutes, significantly improves the crystallinity of the coating layer as evidenced by increase in the sharpness (i.e. decrease of half-intensity width) of hydroxyapatite characteristic peaks.

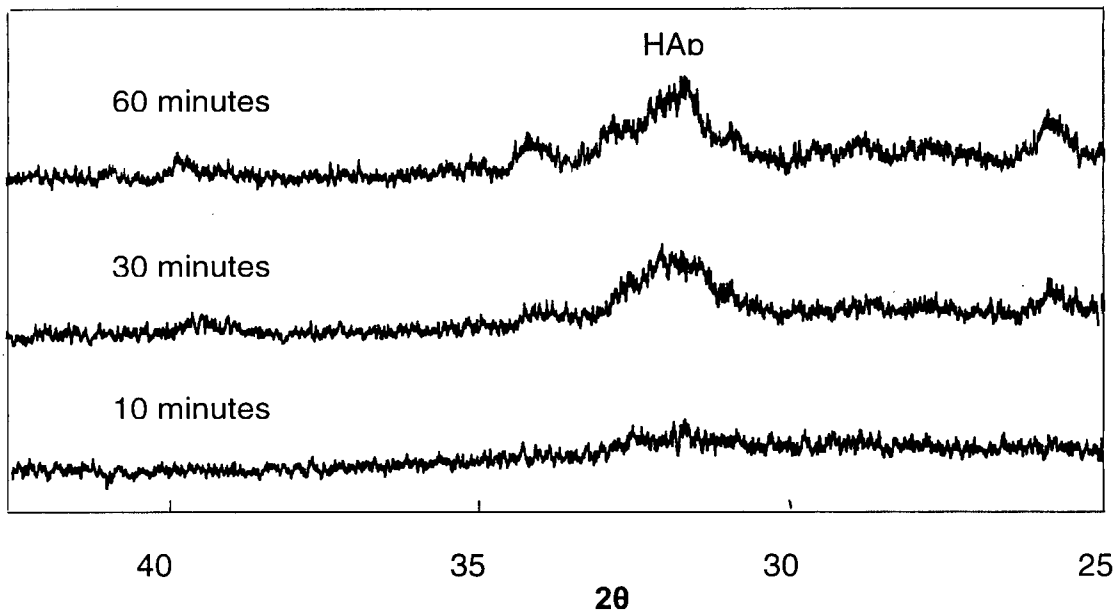


**Figure 5.18** XRD results on thin film coatings fired at 500°C for different time periods.

It appears that the extent of damage of longer-fired films correlates with the sintering time, which in turn increases degree of crystallization, density, stiffness and brittleness of the films. The increased sintering shrinkage produces higher residual stress, and therefore cause further cracking and damage after unbending of coated wires. At the same time, increase in the firing time may result in a better adhesion between the coating and the substrate, as a result of interfacial inter-diffusion between the substrate and the coating [85]. However, due to the relatively low temperature of firing applied here (500°C), this effect is unlikely.

### 5.2.2.2 Stents

The stents evaluated in this work were produced in proprietary process, including the two final steps of surface cleaning (termed "de-oxidation") and edge rounding ("electropolishing"). Figure 5.19 illustrates surface of a stent after the de-oxidation step. 2-8 μm wide grooves are observed on the surface, and a 2-3 μm thick nickel rich layer (evidenced by EDS) covers the interior side of the stent structure after the "de-oxidation" step .

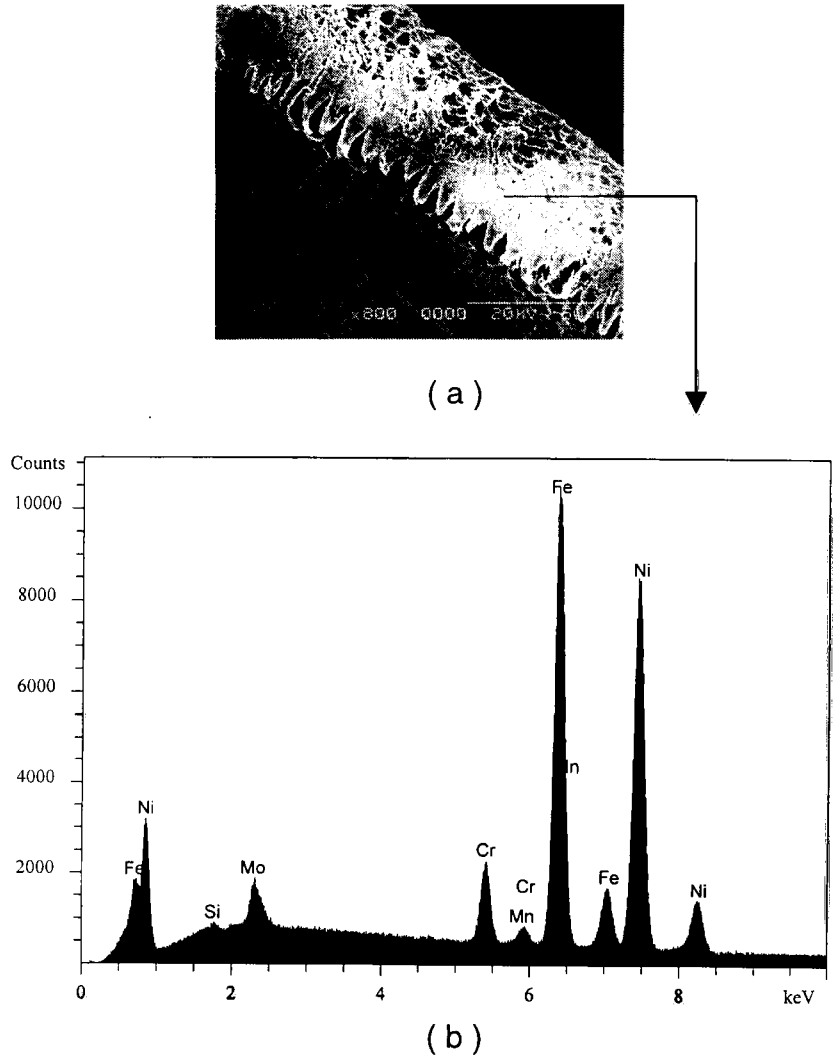


**Figure 5.19** (a) SEM picture of the stent surface obtained after de-oxidizing process, (b) EDS of the ticker layer on the stent surface.

Such stents were dip coated with a withdrawal speed of 14 cm/min with diluted (1M) methanol solution and fired at 500°C for 10 minutes. The colour of the stent surface changed from silver (before coating) to gold (after coating and firing). Figures 5.20a and 5.20b show SEM micrographs of the "de-oxidized" stent surface after coating and firing.

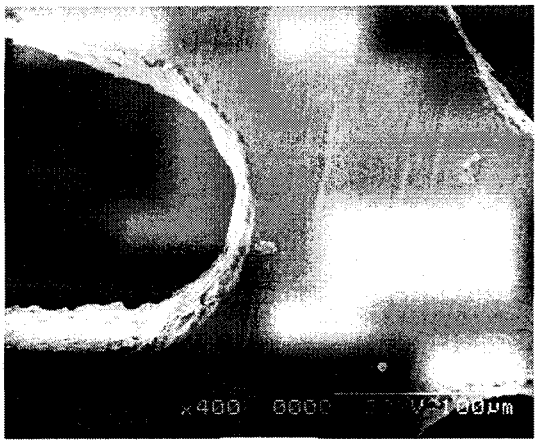


( a )

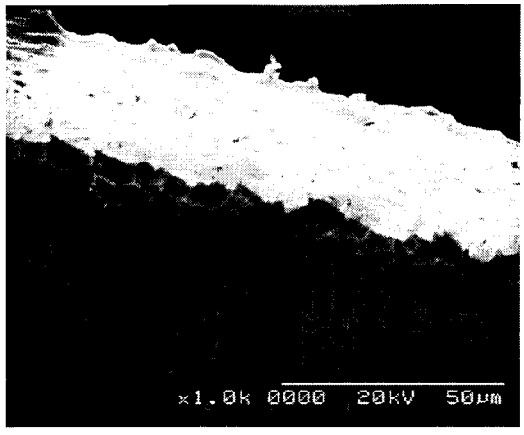


( b )

**Figure 5.20** (a) and (b) show SEM micrographs of the de-oxidize stent surface after coating with dilute methanol solution and fired at 500°C for 10 minutes.

As it can be observed in these two pictures, the coating covers the surface entirely. No microcracking and disintegration or accumulation of coating solution in the U-shaped areas is observed. A thicker coating is observed on the Ni-rich layer present on the interior side of the stent. This effect is due to the rougher surface of these areas, which traps the solution during dip coating. Figures 5.21a and 5.21b show the EDS results of the front and interior surfaces, respectively. The appearance of calcium and phosphorous peaks proves the existence of the coating while higher intensities of these peaks in Fig. 5.21b demonstrates the thicker layer of the coating on the pre-existing Ni-rich layer on the interior surface.

Figures 5.22a-b show the coated stent after expansion with a rapid exchange catheter with a semi-compliant balloon at 10-bar pressure. As it can be observed in Fig. 5.22a no cracking or disintegration is observed on the surfaces of the bar-shaped parts of the

stent structure. Some microcracking and delamination of small areas are observed on the coating as evidenced in Fig. 5.22b. The damaged areas are Ni-rich layers delaminating from the surface due to their loose bonding to the surface and also cracking on the coating due to its larger thickness on the Ni-rich layer.

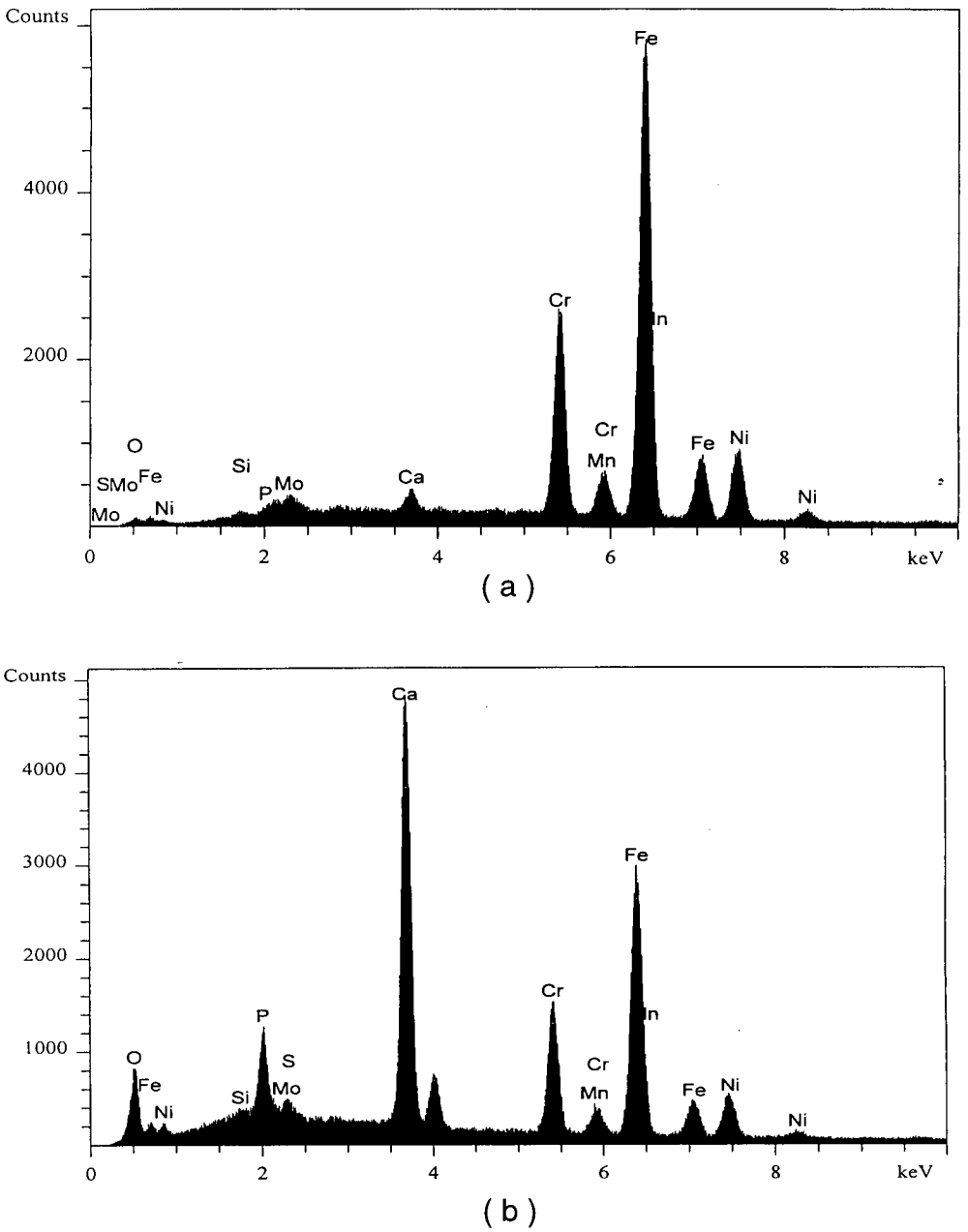


**Figure 5.21** EDS results of the (a) front and (b) interior surfaces of the coated stent structure.

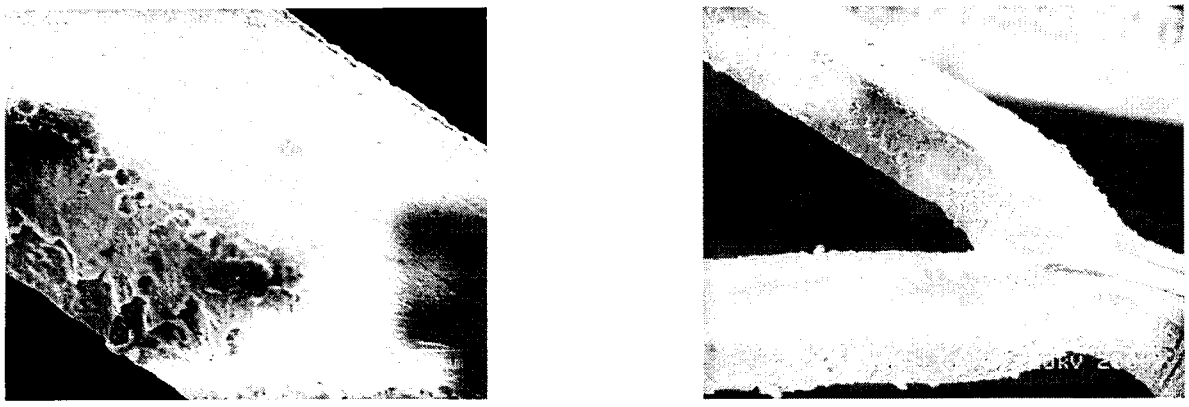

( a ) ( b )

**Figure 5.22** (a-b) SEM pictures of the coated stent after expansion.

Figure 5.23a and 5.23b show the electropolished stent prior and after etching in HCl solution for 10 minutes at 70°C, respectively. As it is evidenced in Fig. 5.23a the outer surfaces of the stent is significantly smoothened after electropolishing, while some surface roughness is observed on the interior surfaces. After etching the samples in HCl for 10 minutes no significant surface roughening on the surfaces is observed.

( a ) ( b )

**Figure 5.23** Electropolished stent (a) prior, and (b) after etching in HCl at 70°C for 10 minutes.

Figure 5.24 shows the picture of the etched sample after coating. Coating shrinkage is observed and therefore a good coverage was not achieved. This effect is due to

inadequate interlocking between the coating and the surface, which results in the accumulation of the solution in the form of droplets and is usually observed on very smooth surfaces. A better coverage was obtained in the interior surfaces due to larger degree of roughness present.

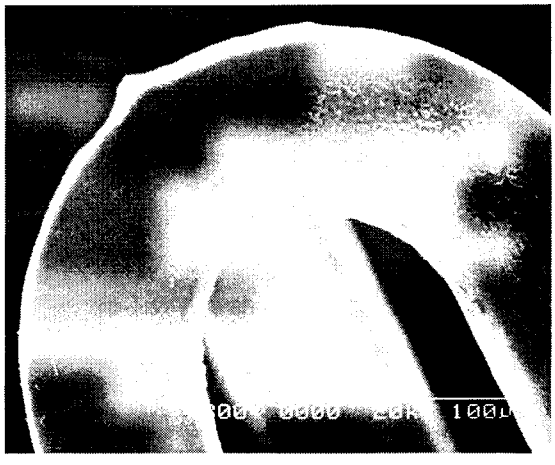

**Figure 5.24** Electropolished stent (a) prior, and (b) after etching in HCl at 70°C for 10 minutes.

# CHAPTER 6

# SUMMARY AND CONCLUSIONS

## 6.1 Summary

In this work the effect of organic (alcohol) solvents on the synthesis and coating properties of a sol-gel hydroxyapatite is investigated. The novel sol-gel technique has been used to process and deposit the coatings. X-ray diffraction analysis, thermal gravimetric and differential thermal analysis, scanning electron microscopy, energy dispersive spectrography and infrared spectroscopy were employed as characterization techniques. Using these techniques, the phase evolution of hydroxyapatite in different solvent systems (methanol, ethanol and propanol) and their effect on microstructure of the calcined gels was investigated. The coating properties are evaluated and discussed. Titanium plates and stainless steel wires were chosen as coating substrates due to their relevance to biomedical industry. Using the knowledge obtained through the course of this study, commercial coronary stents were coated with the sol-gel hydroxyapatite. Deformation characteristics of the coated stents were qualitatively assessed and correlated with the process parameters.

In this sol-gel system triethyl phosphite and calcium nitrate were used as phosphorous and calcium precursors, respectively. In the first step of solution preparation triethyl phosphite was hydrolysed in water, and then mixed with a solution of calcium nitrate in an organic solvent. The mixture of the two solutions was stirred for 30 minutes and aged for 24 hours. Gels were obtained by drying thus prepared solution at 80°C for 24 hours, which were then calcined at 375-545C. Thermal behaviour of the gels and phase evolution of HAp upon heat treatment was monitored.

This study suggests that different organic solvents induce different pathways for HAp formation in the sol-gel system under consideration. The HAp phase evolution depends on the interaction between the solvent and the precursors. Specifically, it is hypothesized that the interaction of the organic molecule of alcohol with calcium can affect the subsequent interaction of calcium-alcohol species with hydrolysed phosphite molecules. According to our observations, impurity phases of calcium phosphate compounds (such as TCP and PP) form in the methanol and propanol-based gels.

These phases further react with other calcium bearing compounds (such as calcium nitrate, calcium oxide and calcium carbonates) to form hydroxyapatite. Due to the good solubility of calcium nitrate in methanol, methyl ligands will easily attach to calcium ion. Because of the large size of thus formed molecules, and their steric hindrance, reaction between calcium and hydrolysed phosphite, necessary to form HAp, would not easily complete. As a result of the incomplete reaction, other (non-HAp) apatite compounds, such as TCP and PP, form along with amorphous apatite intermediate phase. Formation of HAp depends on the reaction between the impurity calcium phosphate compounds, and the remnants of the other impurity phases, such as calcium oxide and calcium carbonates. Due to the low solubility of calcium nitrate in propanol, unreacted calcium nitrate remains in the system, which results in the formation of calcium deficient apatitic compounds. Therefore HAp formation in propanol follows a pathway similar to that in methanol system. In the ethanol system, enough calcium ions are available to interact with hydrolysed phosphite to form an amorphous intermediate apatite phase, which eventually crystallises into HAp. This effect can be attributed to the intermediate solubility of calcium nitrate in ethanol. Therefore it is reasonable to believe that the solubility of calcium nitrate in the organic solvent, and the mechanism of their interaction, will affect the HAp phase evolution pathway in this sol-gel system.

The endothermic DTA peak appeared at the range of 520-550°C in all DTA traces, is assigned to the final HAp formation. The size of this peak was observed to be different the different organic solvents used. A relatively small endothermic peak was observed in the DTA trace at 530°C for ethanol-based sols, compared to the larger respective peaks in DTA results for methanol and propanol-based gels. Based on this observation, it can be concluded that the energy required for formation of hydroxyapatite is different in each solvent system. There is less energy required to form HAp in an ethanol-based system as compared to methanol or propanol-based systems, possibly due to different formation pathways.

Alkyl exchange between solvent and phosphorous alkoxide will take place in this system. This substitution will affect the rate of hydrolysis and condensation reactions leading to different HAp formation pathways in each of the solvent systems while

affecting the morphology of the gel. A continuous, porous structure was observed for the methanol and propanol systems. The large pore size in these systems (~12 μm, on average) can be attributed to evolution of gaseous by-products during the chemical reactions to form HAp. Ethanol-based calcined gel has a particulate, porous structure with pores ranging from 2 to 5 μm in size. The pore size in ethanol system appeared to be smaller compared to those in methanol and propanol systems due to its different HAp formation pathway (crystallization from amorphous phase rather than reaction among impure phases).

Titanium plates were coated with hydroxyapatite through this sol-gel process. In order to increase the adhesion between the coating and the substrate the surfaces of the titanium substrates were roughened using either chemical corrosion or mechanical sandblasting prior to spin coating. The coatings were fired at 500°C for 10 minutes, and characterized using SEM and FTIR. Incubating the substrates in the Simulated Body Fluid (SBF) solution and examining the surface after 7 days of incubation tested the bioactivity of the coatings. All solutions prepared from different organic solvents provided good coverage on the titanium substrate. In the sandblasted surfaces, due to the deep surface irregularities (~10μm) the solution would flow into the cavities and therefore a thicker layer of coating will form which is more susceptible to cracking. This effect increases with the molecular weight of the solvent used, i.e. propanol>ethanol>methanol. Faster desorption of solvents with smaller molecule size and faster decomposition of organic compounds made of these molecules affects the rate of formation and crystallization of HAp. For the similar heat treatment conditions, the HAp rate of formation and crystallization increases with decrease in the alcohol molecule size i.e. methanol>ethanol>propanol, as determined by FTIR. However, no obvious difference between the bioactivity of these coatings was observed after the SBF incubation test.

Medical grade stainless steel wires (316L) were coated with hydroxyapatite using this sol-gel technique. Short period etching in HCl (10 minutes at 70°C) was found as the most suitable procedure for surface roughening of the wires. The wires were then bent, dip coated into the sol, dried and fired at 500°C for 10 minutes. The amount of excess solution trapped in the bent area seems to increase with the organic solvent

molecule size (methanol<ethanol<propanol), especially for the concentrated solutions (2M). The entrapment of the excess solution produced a thicker coating at the bent area, which then cracked and delaminated from the substrate's surface after unbending. Lower concentration of the solution used for coating (1M) decreases this effect. Increasing the firing time of the wires at 500°C to 30 and 60 minutes, promotes crystallization and densification of the coating, while increasing its brittleness.

Stainless steel coronary stents were also used as substrates for this HAp sol-gel process. Stents were obtained after de-oxidizing and electropolishing steps. The rough surface of the deoxidized stents provided enough mechanical interlocking for the coating purposes. A good coverage of the coating was obtained although thicker layers were observed on the nickel-rich layer pre-existing on some surfaces of the stent structure. Cracking and delamination also occurred on this (Ni rich) layer after expansion of the stent while the coating remained intact on other surfaces. The electropolished stent was etched prior to coating in order to produce enough roughness on the surface to provide mechanical interlocking between the coating and the substrate. 10 minutes etching in HCl solution at 70°C did not provide sufficient surface roughness and as a result the coating was accumulated on the surface in the form of droplets, an effect observed in coating very smooth surfaces.

## 6.2 Conclusions

From the data resulting from the present investigation, analysis of the literature data and previous studies, the following conclusions are drawn:

1. Hydroxyapatite (HAp) can be obtained using different organic solvents, such as methanol, ethanol and propanol, in the sol-gel system of triethyl phosphite and calcium nitrate as precursors.

2. Analytical studies of the materials resulting from the process, in particular X-ray diffraction revealed that these different organic solvents induce different phase evolution pathways for the hydroxyapatite, during this sol-gel synthesis. This results in differences in phase composition and crystallinity of the final calcium phosphates. In particular:

2.1. In the methanol system "impurity" calcium phosphate compounds, such as tri-calcium phosphate (TCP) and $Ca_2P_2O_7$ form that will further react with other impurity phases such as calcium oxide and calcium carbonates, to eventually form the hydroxyapatite.

2.2. Propanol system also promotes the formation of impure apatite compounds due to the low solubility of calcium nitrate in propanol, leaving behind unreacted calcium nitrate. Therefore HAp formation follows a mechanism similar to that of the methanol system.

2.3. Due to the complete reaction between calcium ions and hydrolysed phosphite, an amorphous intermediate apatite phase forms in the ethanol-based system that will further crystallize into hydroxyapatite.

2.4. The crystal size of the final hydroxyapatite formed in each of these sol-gel systems follows the order of methanol>propanol>ethanol after heat treatment at 500°C when the samples were removed instantly upon reaching this temperature which is believed to be affected by the HAp formation pathways.

3. As observed in DTA data, the energy required to form hydroxyapatite in different solvent systems follows the order of methanol>propanol>ethanol.

4. SEM observations showed different morphologies for the calcined gels obtained from the different solvent systems. A three dimensional and highly porous structure was observed for the methanol and propanol-derived gels, with the pore size ranging between 2-20 μm. Ethanol-based gel has a particulate structure with much smaller pores (2-5 μm).

5. Titanium plates were spin coated with this sol-gel system.

5.1. Small microcracks (1-2 μm) were observed in the coatings deposited on chemically treated (in 85% phosphoric acid at 50-60°C for 10 minutes) titanium surfaces. The cracks were however much less extensive as compared to plasma sprayed HAp coatings.

5.2. The extent of microcracking increased with the size of the solvent (alcohol) molecule used for sol preparation, for the coatings on sandblasted titanium surfaces. This effect is due to sol accumulation in the cavities of surface irregularities produced by sandblasting, which caused thicker layer formation in these areas.

5.3. Infrared spectroscopy (FTIR) on the surface of coated titanium plates showed the presence of carbonated hydroxyapatite, similar to that of the natural bone.

5.4. FTIR study also revealed that the apatite crystallinity (for the same heat treatment schedule) decreases with the size of the alcohol molecule i.e. methanol> ethanol> propanol, possibly due to the faster resorption of smaller organic species.

5.5. All the obtained coatings were proved to be bioactive through the in-vitro Simulated Body Fluid (SBF) incubation test. Coatings obtained from different solvent systems showed no apparent difference in bioactivity, when tested in SBF (simulated body fluid).

6. Stainless steel wires were bent (to simulate geometry of the stent) and coated with hydroxyapatite through this sol-gel process, with the following results:

6.1. Hydrochloric acid is a suitable agent to roughen the surface of stainless steel wires to enhance its mechanical interlocking with the coating. Both dilute and concentrated HCl are suitable for this purpose.

6.2. Organic solvents with smaller molecular size result in less entrapment of the sol in the bent area of the wire and therefore less cracking and delamination is produced after unbending, as evidenced by SEM observations.

6.3. SEM micrographs show that lower concentration of the solvent (i.e. 1M) reduces the amount of excess solution in the bent area.

6.4. XRD results show that increase in the firing time promotes crystallization of the coating layer. However, more crystalline layer is more prone to cracking under applied stress due to the higher amount of residual sintering strain, and the expected higher stiffness of the coating.

7. Coronary stents were also coated in this so-gel system.

7.1. De-oxidized stents were successfully coated with this sol-gel system. SEM observations confirmed a good coverage of the coating on the stent surface.

7.2. Both EDS and SEM examinations revealed the presence of a thicker coating on nickel-rich layers, pre-existing on some surfaces. This effect is produced due to the larger degree of roughness present on these layers.

7.3. Slight cracking and delamination of the coating was observed after expansion of the stent. This effect was mostly observed on thicker coating present on Ni-rich

layers. Delamination was also occurred due to de-bonding of theses Ni-rich layers from the surface.

7.4. 10 minutes etching of the electropolished stent in HCl solution at 70°C was not sufficient to produce enough surface roughness and as a result the coating solution was accumulated on the surface in the form of droplets, an effect usually observed on very smooth surfaces.

# CHAPTER 7
# RECOMMENDATION FOR FUTURE WORK

The future work should focus on the optimization of the HAp sol-gel coatings on various medical grade substrates such as stainless steel stents. The main challenge in the coating of the stents is to reduce the surface roughening necessary for coating adhesion while maintaining enough adhesion to prevent delamination of the coating after expansion of the stent. The extent of chemical surface preparation (involving surface corrosion), enough to provide mechanical interlocking, should be optimized through examining the coating adhesion to the stent surface. This parameter can also be balanced with coating thickness.

The effects of different dip coating parameters, such as dipping speed, on the quality and thickness of the final coating remains to be investigated. As mechanical properties of the stent should not be affected by the coating and surface preparation procedures, the effect of surface treatment and firing time and temperature on the mechanical properties of stent such as fatigue and wear resistance should be studied.

The rate of coating dissolution into the physiological environment determines the bioactivity of the coating while affecting the coating integrity throughout the stent operation inside the body. Therefore parameters affecting the rate of coating dissolution such as the degree of crystallinity of the coating and also coating thickness should be investigated. Finally, in-vivo and in-vitro bioactivity tests should follow the successful coating procedure.

## NOMENCLATURE

### Latin Symbols

| | |
|---|---|
| ***D*** | crystal size (Eqn 5.4) |
| ***h*** | film thickness (Fig 2.2, Eqn 5.6) |
| ***S*** | stagnation point (Fig 2.2) |
| ***U*** | withdrawal speed (Fig 2.2, Eqn 5.6) |

### Greek Symbols

| | |
|---|---|
| $\gamma_{lv}$ | liquid-vapor surface tension (Eqn 5.6) |
| $\delta$ | boundary layer (Fig 2.2) |
| $\eta$ | viscosity (Eqn 5.6) |
| $\lambda$ | wave length (Eqn 5.4) |
| $\Delta(2\theta)$ | peak width at half maximum intensity (Eqn 5.4) |

### Abbreviation

| | |
|---|---|
| **ACP** | amorphous calcium phosphate |
| **CN** | calcium nitrate |
| **DCP** | monetite, $CaHPO_4$ |
| **DCPD** | dicalcium phosphate dihydrate |
| **HAp** | hydroxyapatite, $Ca_{10}(PO_4)_6(OH)_2$ |
| **OCP** | octacalcium phosphate, $Ca_8H_2(PO_4)_6.5H_2O$ |
| **PP** | $Ca_2P_2O_7$ |
| **SEM** | scanning electron microscope |
| **TCP** | tricalcium phosphate, $Ca_3(PO_4)_2$ |
| **TTCP** | tetra calcium phosphate,$Ca_4P_2O_9$ |
| **XRD** | x-ray diffraction |

## REFERENCES

[1] H. R. Piehler," The Future of Medicine: Biomaterials," MRS bulletin, p. 67-70, Aug. 2000.

[2] L. L. Hench, " Bioceramics: From concept to clinic," J. Am. Ceram. Soc., 74 (7), 1487 (1991).

[3] M. Pinilla, G. Berrocal Jr., R. Ramirez-Camacho, J. Bujan, E. Herrero," Biomaterials in the reconstruction of human middle ear," Mater.Med. Vol.6 (12), 745 (1995).

[4] G. Monticelli, L. Romanini, O. Moreschini," Review on the aseptic of hip replacement failiures," Bioceramics and the Human Body. Proc. Int. Congress Faenza, 2-5 April, CNR-IRTEC;Agenzia Polo Ceramico, 35 (1991).

[5] K. Hing, S. Best, K. Tunner, W. Bonfield, P. Revel, "Biomechanical assessment of bone ingrowth in porous hydroxyapatite," Mater. Med., 8 (12), 731 (1997).

[6] W. Suchanek, and M. Yoshimura, "Processing and properties of hydroxyapatite-based biomaterials for use as hard tissue replacement implants," J. Mater. Res., 13(1), 94 (1998)

[7] K. de Groot, R. G. T. Greesink, C. P. A. T., " Plasma sprayed coatings of hydroxyapatite," J. Biomed. Mater. Res., 21, 1375 (1987)

[8] G. Dewith, and A. J. Corbijin, "Metal fibre reinforced hydroxyapatite ceramics," J. Mater. Sci., 24 (9), 3411 (1989)

[9] F. Z. Cui, Z. S. Luo, Q. L. Feng, "Highly adhesive hydroxyapatite coatings on titanium alloy formed by ion beam assisted deposition," Mater. Med., 8 (7), 403 (1997).

[10] M. Weinlaender, J. Beumer, E. B. Kenny, P. K. Moy, F. Adar, "Raman microprobe investigation of calcium phosphate phases in three commercially available plasma-flamed-sprayed hydroxyapatite-coated dental implants," Mater. Med., 3 (6), 397 (1992).

[11] L. Huang, Y.Han, K. Xu, " Experimental study of fabrication of hydroxyapatite biocoatings by electrochemical deposition and hydrothermal synthesis," J. Chin. Ceram. Soc., 26 (1), 87 (1998).

[12] C. J. Brinker, G. W. Sherer, " Sol-gel science: The physics and chemistry of sol-gel processing," Academic press, Harcout Brace Jovanovich publishers, Boston, San Diego, New York, London, Sydny, Tokyo and Tronto, xiv 908, (1991).

[13] T. Nakamura, "Further advancement of ceramic biomaterial in 21$^{st}$ century is expected by orthopaedic surgeons," Ceram. Jap., 36 (1), 22 (2001).

[14] G. Willmann, " medical grade hydroxyapatite: state of the art," Br. Ceram. Trans., 95 (5), 212 (1996).

[15] G. G. Niederauer, T. D. McGee, R. K. Kudej, "Evaluation of a bioactive ceramic composite as dental implant," Am. Ceram. Soc. Bull., 70 (6), 1010 (1991).

[16] E. Pamula, C. Paluszkiewicz, M. Blazewicz, "Structural changes of carbon fibers in biological environment," Third Euro-Ceram, 3, 125 (1993).

[17] P. Cerrai, G. D. Guerra, M. Tricoli, A. Krajewski, A. Ravaglioli, R. Martinetti," Periodontal membranes from composites of hydroxyapatite and bioresorbable block copolymers," Mater. Med., 10 (10/11), 677 (1999).

[18] I. Ono, " Clinical significance of ceramics in cranio-maxillofacial surgery," Ceram. Jap., 34 (7), 522 (1999).

[19] T. Yamamuro, "AW glass-ceramics in spinal repair," Bioceramics. Proc.8th Int.Symp.on Ceramics in Medicine. Florida, 8, 123 (1995)

[20] Racquel Z. Legeros, " Biodegradation and bioresorption of calcium phosphate ceramics," Chemical Materials, 14, 65-88, (1993).

[21] H. S. Cheung, and D. J. McCarty," Mitogenesis induced by calcium containing crystals. Role of intracellular dissolution," Experiment. Cell. Res., 157, 63 (1985).

[22] Merriam-Webster Dictionary on-line,( www.m-w.com).

[23] L. C. Chow, S. Takagi, P. Costantino, and C. Friedman, "Self-setting calcium phosphate cements," Mater. Res. Soc. Symp. Proc., 179, 3 (1991)

[24] H. Aoki, " Science and medical applications of hydroxyapatite," JAAS, Tokyo, (1991)

[25] M. Shrkhanzadeh, and M. Azadegan, " Hydroxyapatite particles prepared by electrocrystallization from aqueous electrolytes," Matter, Letter, 15, 392 (1993)

[26] M. Aizawa, K. Itatani, F. S. Howell, and A. Kishioka, " Some properties of carbonate-containing hydroxyapatite powder prepared by spray-pyrolysis technique using urea as a foaming agent," J. Ceram. Soc.. Jpn., 103, 1214 (1995).

[27] H. Lu, and Y. C. Zhou, " preparation and mechanical properties of dense polycrystalline hydroxyapatite through freeze-drying," J. Mater. Sci. Mater. Med., 9 (10), 583 (1998).

[28] E. Lerner, S. Sarig, and R. Azoury, "Enhanced maturation of hydroxyapatite from aqueous solutions using microwave irradiation," J. Mater. Sci. Mater. Med., 2 (3), 138 (1991).

[29] M. Toriyama, A. Ravagliolli, A. Krajewski, G. Celohi, and A. Pincatelli, " Synthesis of hydroxyapatite-based powder by mechano-chemical method and their sintering," J. Eur. Ceram. Soc., 16 (4), 429 (1996)

[30] M. G. S. Murray, J. Wang, C. B. Ponton, and P. M. Marquis, " Improvement in processing of hydroxyapatite ceramics," J. Mater. Sci., 30 (12), 3061 (1995)

[31] J. Li, B. Fartash, and L. Hermansson, " High strength ceramics with potential bioactivity," Interceram. , 39 (6), 20 (1990)

[32] K. Ioku, T. Noma, N. Ishizawa, and M. Yoshimura, "Hydrothermal synthesis and sintering of hydroxyapatite powders with $Si_3N_4$ whiskers dispersion," J. Ceram. Soc. Jpn. Int. Ed., 98 (12), 1337 (1990).

[33] A. J. Ruys, S. A. Simpson, and C.C. Sorrell, " Thixotropic casting of fibre-reinforce ceramic-matrix composites," J. Mater. Sci. Lett., 13 (18), 1323 (1994).

[34] Y. Fang, D. M. Roy, J. Cheng, R. Roy, and D. K. Agrawal, "Microwave sintering of hydroxyapatite-based composites," Ceram. Trans., 36, 397 (1993).

[35] T. K. Chaki, and P.E. Wang," Densification and strengthening of silver-reinforced hydroxyapatite matrix composites prepared by sintering," J. Mater. Sci. Mater. Med., 5 (8), 533 (1994).

[36] W. R. Lace field, "an introduction to Bioceramics," edited by L. L. Hench and J. Wilson, Adv. Ser. Ceram., Vol. 1, World scientific publishing Ltd., (1993)

[37] J. C. Knowles, K. Gross, C. C. Brendt, and W. Bonfield, "Structural changes of thermally sprayed hydroxyapatite investigated by Rietveld analysis," Biomaterial, 17 (6), 639 (1996).

[38] K. Van Dijk, H. G. Schaeken, J. G. C. Wolke, and J. A. Jansen,"Influence of annealing temperature on RF magnetron sputtered calcium phosphate coatings," Biomaterials, 17 (4), 405 (1996).

[39] A. M. Ektasabi," Ion-beam processing of Bio-ceramics," Nucl. Instrum. Methods Phys. Res., B99, 610 (1995).

[40] Y. Fujishiro, T. Sato, and A Okuwaki, " Coating of hydroxyapatite on metal plates using thermal dissociation of calcium-EDTA chelate in phosphate solutions under hydrothermal conditions," J. Mater. Sci. Mater. Med., 6 (3), 172 (1995).

[41] M. Shirkhanzadeh, M. Azadegan, V. Stad, and S. Schreyer, "Fabrication of pure hydroxyapatite and fluorinated-hydroxyapatite coatings by electrocrystallization," Mater. Letter, 18, 211 (1994).

[42] B. E. Tucker, C. M. Cottel, R. C. Y. Auyeung, M. spector, and G. H. Nancollas, "pre-conditioning and dual constant composition dissolution kinetics of pulsed laser deposited hydroxyapatite thin films on silicon substrate," Biomaterials, 17, 631 (1996).

[43] F. J. Guild, and W. Bonfield, " Predictive modeling of hydroxyapatite polyethylene composite," Biomaterials, 14 (13), 985 (1993).

[44] C. Moorlag, M. Sc. Thesis, "Chemically bonded sol-gel ceramics: A study of alumina-phosphate reaction products," Department of Metals and Materials Engineering, University of British Columbia, August 2000.

[45] A. Jillavenkatesa, and R. A. Condrate SR, " Sol-gel processing of hydroxyapatite," J. Maters. Sci., 33, 4111 (1998).

[46] P. Layrelle, A. Ito, and T. Tateishi, " Sol-gel synthesis of amorphous calcium phosphate and sintering into microporous hydroxyapatite Bioceramics," J. Am. Ceram. Soc., 81 [6], 1421 (1998).

[47] Y. Masuda, K. Matubara, and S. Sakka, "Synthesis of hydroxyapatite from metal alkoxides through sol-gel technique," J. Ceram. Soc. Jpn, 98, 1266 (1990).

[48] H. Takahashi, M. Yashima, M. Kakihana, and M. Yoshimura, "Synthesis of stoichiometric hydroxyapatite by a "gel" route from the aqueous solution of citric acid and phosphonoacetic acid," Eur. J. Solid State Inorg. Chem., t. 32, 829 (1995).

[49] G. Kordas and C.C. Trapalis, " Fourier transform and multi dimensional EPR spectroscopy for the characterization of sol-gel derived hydroxyapatite," J. Sol-gel Sci. and Technol., 9, 17 (1997).

[50] J. Livage, P. Barboux, M. T. Vandenborre, C. Schmtz, and F. Taulelle, " Sol-gel synthesis of phosphates," J. non-Crystl. Solids, 147&148, 18 (1992).

[51] C. S. Chai, K. A. Gross, B. Ben-Nissan, "Critical ageing of hydroxyapatite sol-gel solutions," Biomaterials, 19, 2291 (1998).

[52] A. Jillavenkatesa, D. T. Hoelzer, R. A. Condrate, SR., " An electron microscopy study of the formation of hydroxyapatite through sol-gel processing," J. Maters. Sci., 34 4821 (1999).

[53] W. Weng, L. Haung, and G. Han, " The alkoxide sol-gel process in the calcium phosphate system and its applications," Appl. Organometal Chem., 13, 555 (1999).

[54] A. Deputla, W. Lada, T. Olczak, A. Borello, C. Alvani, and A. di Bartolomeo, "preparation of spherical powders of hydroxyapatite by sol-gel process," J. non-crystl. Solids, 147/148, 537 (1992).

[55] W. Weng. J. L. Baptista, " A new synthesis of hydroxyapatite," J. Eur. Ceram. Soc., 17, 1151 (1997).

[56] D. M. Liu, T. Trozynski, W. Tseng, Biomaterials, "Water-based sol-gel synthesis of hydroxyapatite: process development," 22, 1721 (2001).

[57] D. M. Liu, D. Hakimi Mehr, T. Troczynski, " Effect of hydrolysis on the phase evolution of water-based sol-gel hydroxyapatite and its application to bio-coating," J. Mater. Sci. Mater. Med., To be published.

[58] L. D. Piveteau, M. I. Girona, and L. Schalpbach, " thin films of calcium phosphate and titanium dioxide by sol-gel route: a new method for coating medical implants," J. Mater. Sci. Mater. Med., 10, 161 (1999).

[59] D. B. Haddow and P. F. James, J. Sol-gel Sci. and Tchnol., " Sol-gel derived calcium phosphate coatings for biomedical applications," 13, 261 (1998).

[60] W. Weng and J. L. Baptista," Sol-gel derived porous hydroxyapatite coatings," J. Mater. Sci. Mater. Med., 9, 159 (1998).

[61] C. S. Chai, B. Ben-Nissan, " Bioactive nanocrystalline sol-gel hydroxyapatite," J. Mater. Sci. Mater. Med., 10, 465 (1999).

[62] K. Hwang, Y. Lim, " Chemical and structural changes of hydroxyapatite films by using a sol-gel method," Surface Coatings Technology, 115, 172 (1999).

[63] K. A. Gross, C. S. Chai, G. S. K. Kannangara, B. Ben-Nissan, and L. Hanley, " Thin hydroxyapatite coatings via sol-gel synthesis," J. Mater. Sci. Mater. Med., 9, 839 (1998).

[64] K. Hwang, J Song, B. Kang, and Y. Park, "Sol-gel derived hydroxyapatite films on alumina substrates," Surface and coatings Technology, 123, 252 (2000).

[65] C. M. Lopatin, V. Pizziconi, T. L. Alford, and T. Laursen, " Hydroxyapatite powders and thin films prepared by sol-gel technique," Thin Solid Films, 326, 227 (1998).

[66] D. A. Bloom, R. V. Clayman, and E. Mcdougal," stents and related terms: A brief history," Urology, 54, 767 (1999).

[67] O. F. Bertrand, MD, R. Sipehia, PhD, R. Mongrain, PhD, J. Rodes, MD, J. C. Tardif, MD, L. Bilodeau, MD, G. Cote, MD, FACC, and M. G. Bourassa, MD, FACC, " Biocompatibility aspects of new stent technology," J. Am. Coll. Cadiol., 32, 562 (1998).

[68] U. O. Hafeli, M. C. Waburton, and U. Landau, " Electrodeposition of radioactive rhenium onto stents to prevent restenosis," Biomaterials, 19, 925 (1998).

[69] D. Holmo, R. Vietstra, H.. Smith, G. Vetrovec, K. Kent, M. Clowly, D. Faxon, A. Gruentzig, S. Kelsey, K. Detre, M. Van Raden, and M. Mock, "Restenosis after PTCA: A report from the PTCA registry of the national heart, lung and blood institute," Am. J. Cardiol., 53, 77C (1984).

[70] W. Casscels, D. Engler, and J. T. Willerson, " mechanisms o restenosis," Texas Heart Inst. J., 21, 68 (1994).

[71] W. Van der Giessen, A. Lincoff, R. Schwartz, et. al., " Marked inflammatory sequlae to implantation of biodegradable and Nonbiodegradable polymers in porcine coronary arteries," Circulation, 94, 1690 (1996).

[72] I. De Sheerder, K. Wilczek, E. Verbeken, et. al., "Biocompatibility of polymer-coated oversized metallic stents implanted in normal porcine coronary arteries," Atherosclerosis, 114, 105 (1995).

[73] A. Fortaine, K. koelling, J. Clay, " Decreased platelet adherence of polymer coated tantalum stents," J. Vasc. Interv. Radiol, 5, 567 (1994).

[74] E. Recharia, M. Fishbren, T. defrance, M. Nakemura, F. Litvak, N. Eigler, "Vascular injury triggered by temporary and permanently implanted polyurethane coated and uncoated stents in rabbit carotid," Circulation, 94, I-81 (1996).

[75] A. Lincoff, J. Frust, S. Ellis, R. Tuch, E. Topol, " Substantial local delivery of dexamethasone by a novel intravascular eluting stent to prevent restenosis in the porcine coronary injury model," J. Am. Coll. Cardiol., 29, 808 (1997).

[76] J. Baker, J. Horn, V. Nikolaychik, N. Kipshize, "Fibrin stent coatings" edited by V. Sigwart, Endoluminal stenting, London, Philadelphia, Toronto, Sydney, Tokyo; WB Saunders, 84 (1996).

[77] C. Stenefanidis, K. Toutouzas, C. Vlachopoulos, et. al., "Stents wrapped in autologous vein, an experimental study," Circulation, 28, 1039 (1996).

[78] T. Susawa, K. Shiraki, Y. Shimizu, "Biodegradable intracoronary stents in adult dogs," J. Am. Coll. Cardiol, 21, 483A (1993).

[79] J. Bier, P. Zalesky, H. Sasleen, D. Williams, "A new biodegradable intravascular stent in vitro assessment of hemodynamic and morphometric characterization," Circulation, 84, II-197 (1991).

[80] D. M. liu, H. M. Chou, and J. D. Wu, " Plasma-sprayed hydroxyapatite coatings: Effect of different calcium phosphate ceramics," J. mater. Sci. mater. Med., 5, 147 (1994).

[81] F. S. Shieu, M. J. Deng, K. C. Lin, J. C. Wong, "Effect of surface pre-treatment on the adherence of porcelain enamel to a type 316L stainless steel," J. Mater. Sci., 34, 5265 (1999).

[82] D. M. Liu, T. Troczynski, and W. J. Tseng, " Aging effect on the phase evolution of ware-based sol-gel hydroxyapatite," Biomaterials, To be published.

[83] J. Livage, M. Henry, and C. Sanchez, "Sol-gel chemistry of transition metal oxides," prog. Solid St. Chem., 18, 259 (1988)

[84] K. de Groot, R. G. T. Greesink, C. P. A. T. klein and Serekian, "Plasma-sprayed coatings of hydroxyapatite," J. Biomed. Mater. Res., 21, 1375 (1987).

[85] X. Miao, and B. ben-Nissan, " Microstructure and properties of zirconia-alumina nanoaluminate sol-gel coatings," J. Mater. Sci., 35, 497 (2000).

## APPENDIX I

The following is a comparison of the ion concentrations of the simulated body fluid (SBF) and human blood plasma (HBP).

| Ions | Conc. In SBF (mM) | Conc. In HBP (mM) |
|---|---|---|
| $Na^+$ | 142.0 | 142.0 |
| $K^+$ | 5.0 | 5.0 |
| $Mg^+$ | 1.5 | 1.5 |
| $Ca^+$ | 2.5 | 2.5 |
| $Cl^-$ | 147.0 | 103.0 |
| $HCO_3^-$ | 4.0 | 27.0 |
| $HPO_4^{2-}$ | 1.0 | 1.0 |
| $SO^{2-}$ | 0.5 | 0.5 |

## APPENDIX II

Standard X-ray diffraction data for hydroxyapatite.

9- 432 JCPDS-ICDD Copyright (c) 1991 Rad.= 1.54056 Quality: i

Ca (PO ) (OH)
5 4 3

Calcium Phosphate Hydroxide

Hydroxylapatite, syn

Rad: CuKal Lambda: 1.54056 Filter: d-sp: D.S. -114.6
Cutoff: Int: I/Icor:
Ref: de Wolff, Technisch Physische Dienst, Delft, Netherlands, JCPDS Grant-in-Aid Report

Sys: Hexagonal S.G.: P63/m (176)
a: 9.418 b: c: 6.884 A: C: .7309
A: B: C: Z: 2 mp:
Ref: Ibid.

Dx: 3.15 Dm: 3.08 SS/FOM: F30=54(.016,35)

ea: nwB: 1.651, ey: 1.644, Sign: - 2V:
Ref: Dana's System of Mineralogy, 7th Ed., 2 879

Color: Sea-green, asparagus-green, bluish green, grayish green also, violet, violet-blue, amethystine, sometimes colorless, pale greenish white, gray, brown, flesh red, rose-red, clear blue
Sample obtained following the procedure indicated by Hodge et al., Ind. Eng. Chem. Anal. Ed., 10 156 (1938). CAS no.: 1306-06-5. I/I1 are peak values from a pattern which shows slight broadening of prism reflections. Validated by calculated data 24-33. Apatite group, apatite subgroup. PSC: hP44. To replace 34-10. Mwt: 502.32. Volume[CD]: 528.80.

| 2-theta | Int. | h k l |
|---|---|---|
| 10.820 | 12 | 1 0 0 |
| 16.841 | 6 | 1 0 1 |
| 18.785 | 4 | 1 1 0 |
| 21.819 | 10 | 2 0 0 |
| 22.902 | 10 | 1 1 1 |
| 25.354 | 2 | 2 0 1 |
| 25.879 | 40 | 0 0 2 |
| 28.126 | 12 | 1 0 2 |
| 28.966 | 18 | 2 1 0 |
| 31.773 | 100 | 2 1 1 |
| 32.196 | 60 | 1 1 2 |
| 32.902 | 60 | 3 0 0 |
| 34.048 | 25 | 2 0 2 |
| 35.480 | 6 | 3 0 1 |
| 39.204 | 8 | 2 1 2 |
| 39.818 | 20 | 3 1 0 |
| 40.452 | 2 | 2 2 1 |
| 42.029 | 10 | 3 1 1 |
| 42.318 | 4 | 3 0 2 |
| 43.804 | 8 | 1 1 3 |
| 44.369 | 2 | 4 0 0 |
| 45.305 | 6 | 2 0 3 |
| 46.711 | 30 | 2 2 2 |
| 48.103 | 16 | 3 1 2 |
| 48.623 | 6 | 3 2 0 |
| 49.468 | 40 | 2 1 3 |
| 50.493 | 20 | 3 2 1 |
| 51.283 | 12 | 4 1 0 |
| 52.100 | 16 | 4 0 2 |
| 53.143 | 20 | 0 0 4 |
| 54.440 | 4 | 1 0 4 |
| 55.879 | 10 | 3 2 2 |
| 57.128 | 8 | 3 1 3 |
| 58.073 | 4 | 5 0 1 |
| 59.938 | 6 | 4 2 0 |
| 60.457 | 6 | 3 3 1 |
| 61.660 | 10 | 2 1 4 |
| 63.011 | 12 | 5 0 2 |
| 63.443 | 4 | 5 1 0 |
| 64.078 | 13 | 3 0 4, 3 2 3 |
| 65.031 | 9 | 5 1 1 |
| 66.386 | 4 | 4 2 2, 4 1 3 |
| 69.699 | 3 | 5 1 2 |
| 71.651 | 5 | 4 3 1, 4 0 4 |
| 72.286 | 4 | 5 2 0, 2 0 5 |
| 73.995 | 7 | 4 2 3 |
| 75.022 | 3 | 3 2 4, 6 0 2 |
| 75.583 | 9 | 2 1 5 |
| 76.154 | 1 | 4 3 2 |
| 77.175 | 11 | 5 1 3 |
| 78.227 | 9 | 5 2 2 |

Strong lines: 2.81/X 2.78/6 2.72/6 3.44/4 1.84/4 1.94/3 2.63/3 2.26/2